Journal Pre-proofs

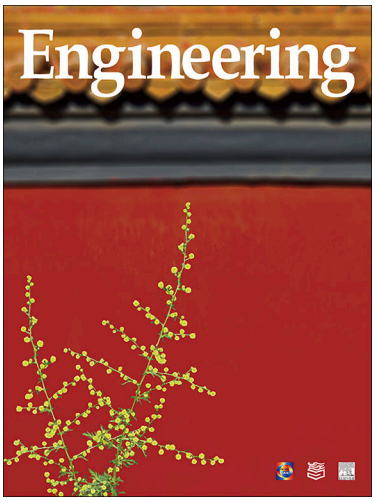

Article

Synergism Between Electron Donors and Microbes Toward Highly Efficient Denitrification with Minimal Sludge Yield

Jing Zhao, Yunjie Liao, Yuting Wang, Qinghua Ji, Ruiping Liu, Huijuan Liu

PII: S2095-8099(26)00181-5
DOI: https://doi.org/10.1016/j.eng.2026.03.014
Reference: ENG 2307

To appear in: *Engineering*

Received Date: 22 September 2025
Revised Date: 18 February 2026
Accepted Date: 2 March 2026

Please cite this article as: J. Zhao, Y. Liao, Y. Wang, Q. Ji, R. Liu, H. Liu, Synergism Between Electron Donors and Microbes Toward Highly Efficient Denitrification with Minimal Sludge Yield, *Engineering* (2026), doi: https://doi.org/10.1016/j.eng.2026.03.014

Synergism Between Electron Donors and Microbes Toward Highly Efficient Denitrification with Minimal Sludge Yield

Jing Zhao, Yunjie Liao, Yuting Wang, Qinghua Ji*, Ruiping Liu, Huijuan Liu

Center for Water and Ecology, State Key Laboratory of Regional Environment and Sustainability, School of Environment, Tsinghua University, Beijing 100084, China

*Corresponding author
E-mail address: qhji@tsinghua.edu.cn (Q. Ji)

Abstract

Hydrogen (H_2), formate, and acetate are effective electron donors for denitrification; however, their interactions with microflora and their impacts on sludge production remain poorly understood. In this study, integrated mixed- and pure-culture experiments were conducted to systematically elucidate how these electron donors and microbes collectively regulate denitrification and sludge formation. Mechanistic insights were further elucidated using metagenomics-based metatranscriptomics methods. In mixed culture reactors, H_2 and formate share similar microbial communities, dominated by *Paracoccus pantotrophus* (60.4%–70.0%). In contrast, acetate-driven denitrification was primarily facilitated by *Pseudomonas aeruginosa* (42.3%) and *Pseudomonas stutzeri* (39.1%), which achieved the highest denitrification rate of 142.3 $mg_N \cdot (L \cdot h \cdot OD_{600})^{-1}$. Metagenomics-based metatranscriptomics identified *Pseudomonas aeruginosa* as the main contributor to denitrification, a finding validated by pure-culture experiments. Notably, in the pure-culture experiment, *Pseudomonas aeruginosa* demonstrated superior denitrification performance with lower acetate demand (0.56 $g_{COD} \cdot g_N^{-1}$) and lower biomass yield (OD_{600} 0.20 vs 0.54). Support vector machine analysis further indicated that *Pseudomonas* is widely distributed in wastewater treatment plants globally, and that acetate is the most efficient electron donor for denitrification. These results highlight that the combination of acetate and *Pseudomonas aeruginosa* is a promising strategy for achieving high efficiency with minimal sludge production in wastewater treatment plants.

Keywords

Pseudomonas aeruginosa, Denitrification, Electron donor, Meta-omics, Low-sludge generation

1. Introduction

The discharge of nitrogen-rich wastewater from industrial and agricultural activities has become a global environmental concern [1,2]. Excess nitrate (NO_3^-) contamination leads to eutrophication, deteriorates water quality, and disrupts aquatic ecosystems, thereby threatening biodiversity and human health [3,4]. The current denitrification strategies primarily involve physicochemical and biological approaches [5]. Physicochemical methods often require the addition of highly efficient catalysts, which may pose the risk of secondary environmental pollution and significantly increase treatment expense [6]. In contrast, the bio-denitrification process has gained increasing attention owing to its cost-effectiveness, minimal byproduct generation, operational reliability, and environmental compatibility [6,7].

WWTPs play a critical role in nitrogen removal through the bio-denitrification process, traditionally relying on heterotrophic denitrification, in which organic carbon sources (e.g., acetate) serve as electron donors to facilitate microbial nitrate reduction [8]. However, this process faces significant limitations, including overdosing of carbon sources in response to fluctuating NO_3^--N concentrations, which elevates operational costs, enhances greenhouse gas (GHG) emissions, particularly CO_2 and N_2O, and exacerbates sludge production [9–11]. Sludge disposal alone accounts for 49%–53% of WWTP operational expenses and contributes substantially to carbon emissions, ranging from 0.3 to 680 $gCO_2eq \cdot m^{-3}$ [12,13]. Alternatively, H_2-driven autotrophic denitrification has recently attracted interest as a potential substitute because it eliminates the need for organic carbon supplementation, is clean and non-toxic, and markedly reduces sludge yield [1, 14]. Despite these benefits, its application remains constrained by its relatively low nitrogen-removal efficiency and operational safety, limiting its widespread implementation [15]. Thus, denitrification strategies that achieve high nitrogen removal efficiencies while minimizing sludge production are urgently required.

Recent studies have indicated that electron donors and microbes play a decisive role in denitrification [16,17]. Electron donors can alter microbial community structure and metabolic patterns, as observed in *Pseudomonas* and *Thauera*, which are dominant in acetate-fed reactors [17], whereas *Hydrogenophaga* preferentially utilize H_2 [18]. Moreover, electron donors and microbial consortia regulation can reduce cell synthesis, thereby minimizing sludge production in wastewater treatment systems [19–21]. Bacteria constitute the main component of activated sludge [21]. This implies that denitrification efficiency and sludge yield are co-regulated by the type of electron donor and microbial metabolism. However, systematic investigations

into these interactions are limited. A deeper understanding of how electron donors and microorganisms jointly affect deni[Journal Pre-proofs]gies for WWTPs.

H_2 and acetate are widely used for autotrophic and heterotrophic denitrification, respectively [10,14]. Formate, a ubiquitous one-carbon compound in anaerobic environments [22], is another promising electron donor for denitrification due to its excellent storage and transport properties, which warrant further investigation [23]. To systematically assess the effects of electron donors and functional denitrifying microbes on nitrogen removal and sludge generation, we designed a study (Fig. 1) that integrated microbial metabolic pathway analysis with denitrification performance. First, in mixed-culture experiments, we investigated how different electron donors affect the microbial community structure and denitrification rates. Machine learning was applied to visualize the distribution of dominant denitrifying genera (e.g., *Paracoccus* and *Pseudomonas*) and to identify how key operational parameters influence the microbial community in full-scale WWTPs. To further elucidate the molecular metabolic pathway of electron donor utilization, we conducted a metagenomics-based metatranscriptomics analysis [24] to quantify the transcription levels of the dominant genes in the mixed-culture experiment. Subsequently, a pure-culture experiment was performed to validate the optimal pairing of electron donor and microbes for achieving high-efficiency denitrification with minimal sludge yield. Finally, a multi-dimensional evaluation was conducted to propose a practical and scalable denitrification strategy applicable to full-scale WWTPs. By optimizing both electron donor selection and microbial composition, this study aimed to provide valuable insights into the design of efficient, low-carbon-footprint denitrification systems that minimize sludge generation, thereby supporting the global transition toward sustainable wastewater treatment.

2. Materials and Methods

2.1 Mixed-culture denitrification experiment design

Batch tests were conducted to evaluate the denitrification potential of various electron donors in a mixed-culture system. $NaNO_3$ was used as the nitrate source, and CH_3COONa, HCOONa, and H_2 served as electron donors for denitrification, respectively. The experiments involving CH_3COONa, HCOONa, and H_2 were conducted in parallel. For the H_2-driven denitrification, CO_2 was supplied along with H_2 at a 2:1 (H_2: CO_2) ratio to provide an inorganic carbon source for microbial biosynthesis [25]. All experiments were performed in triplicate using 120 mL serum bottles (Fig. 1). Each bottle contained 0.5 mL of inoculum (OD_{600} of approximately 0.5) and 50 mL of the growth medium.

The inoculum was obtained from a lab-scale autotrophic denitrification reactor (Beijing, China), which was continuously fed with a mixed gas (H_2: CO_2 at a 2:1 ratio). The growth medium was prepared in demineralized water with the following composition per liter: 3 g KH_2PO_4, 5.8 g K_2HPO_4, 0.09 g $MgCl_2{\cdot}6H_2O$, and 0.023 g $CaCl_2{\cdot}2H_2O$, formulated to minimize interference from extraneous nitrogen and carbon sources. Additionally, 10 mL of Wolin's vitamin solution (Table S1 in Appendix A) and 10 mL of Wolin's mineral solution (Table S2 in Appendix A) were added per liter of growth medium. Before inoculation, the serum bottles containing the growth medium were purged with argon (Ar) gas for 30 min, sealed with a butyl rubber septum, and autoclaved at 121 ℃ for 15 min. Sterile solutions of $NaNO_3$, formate, acetate, as well as H_2–CO_2 gas, were prepared separately using 0.22 μm membrane filtration. After cooling the growth medium to room temperature, the nitrate solution, electron donor solution (containing the same electron equivalents), and inoculum were aseptically injected into the reactor using syringes to initiate the experiment. All reactors were incubated at 37 ℃ with shaking at 100 $r{\cdot}min^{-1}$. The only variable among the reactors used in the mixed-culture experiment was the type of electron donor.

During the experiment, liquid samples (0.5 mL) were collected periodically to measure the OD_{600} and determine the concentrations of nitrate, nitrite, formate, and acetate. The volume of gas was measured using a syringe. The sampling frequency was adjusted according to the reaction rate, with more frequent sampling during the rapid phases and less frequent sampling during the slower phases. Microbial samples (10 mL) were collected at the end of the experiment (54 h), when denitrification was complete in all the reactors. Samples for EPS analysis were also collected at this point. The denitrification rate ($mg_N \cdot (L{\cdot}h{\cdot}OD_{600})^{-1}$) was calculated based on the time-dependent decrease in nitrate concentration, normalized to biomass density (OD_{600}).

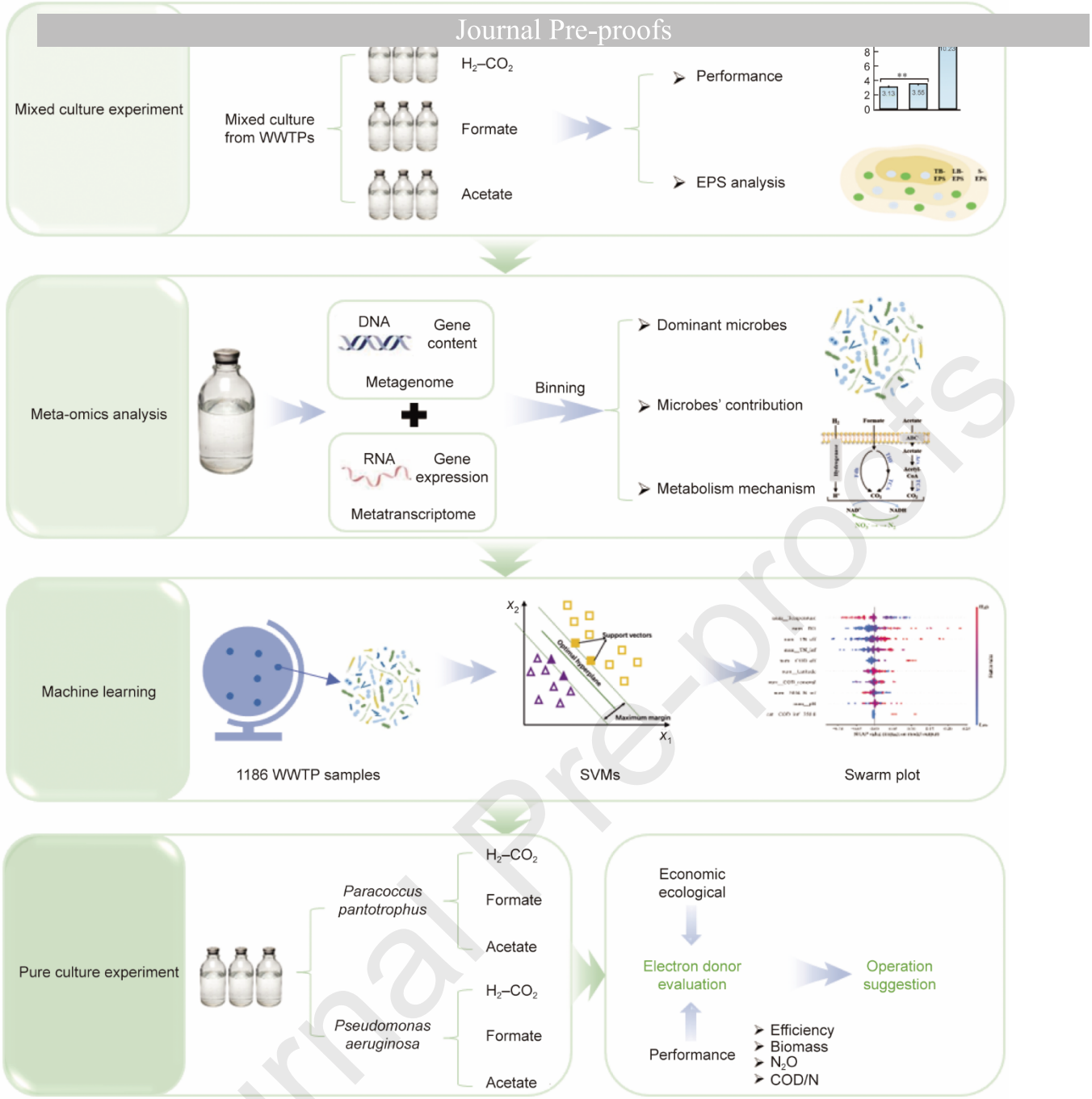

Fig. 1. The setup for the various experiments.

2.2 16S rRNA gene amplicon sequencing, metagenome, metatranscriptome, and bioinformatics analyses

Microbial samples (10 mL) were collected aseptically using sterile syringes at the end of the mixed-culture experiment (54 h) and placed in RNase-free tubes. The samples were centrifuged at 10 000 $r \cdot min^{-1}$ at 4 °C for 15 min, after which the precipitate was collected and stored at –80 °C for further analysis. The DNA and RNA were extracted using the FastDNA SPIN Kit for soil (MP Biomedicals, USA) and TRIzol reagent (Invitrogen, USA), respectively, following the manufacturers' protocols [26]. The samples were then sent to Majorbio Bio-Pharm Technology Co., Ltd. (China) for further analysis.

To characterize the microbial communities and gene content across reactors supplied with H_2, formate, or acetate as electron donors in the mixed-culture experiment, 16S rRNA gene amplicon and metagenomic sequencing were performed. The quality of the extracted DNA was verified by 1% agarose gel electrophoresis. 16S rRNA gene amplicon sequencing was used to profile the microbial community composition, whereas metagenomic analysis of the same DNA extracts revealed differences in gene content across different electron donors. A paired-end library was constructed using the NEXTFLEX™ Rapid DNA-Seq kit (Bio Scientific, USA) and then sequenced on an Illumina HiSeq Xten using HiSeq X Reagent Kits according to the manufacturer's instructions. Sequences with a length ≥ 1000 bp after assembly were binned using Metabat (version 2.12.1). All binned boxes were clustered, and dRep (version 2.2.9) was used to remove duplicate metagenome-assembled genomes

(MAGs). The taxonomic classification of the MAGs was performed using GTDB-Tk (version 2.3.0), and the corresponding phyl

A metatranscriptome was used to characterize the gene transcripts. Metagenomics-based metatranscriptomics analysis was employed to quantify gene transcription levels to ensure accurate assessment of gene transcription and microbial contributions [24]. This analysis was referred to as the metagenomics task (raqo_8fo1167e7utuvak051a8nm). A schematic showing the distinctions between the metagenome, metatranscriptome, and metagenome-based metatranscriptome is shown in Fig. S2 in Appendix A. Sequencing was performed by Majorbio Bio-Pharm Technology Co., Ltd. (China) on an Illumina HiSeq platform [27].

2.3 WWTP samples and an explainable machine learning method

A global dataset of 1186 WWTP microbial samples, along with associated operational parameters, was obtained from a previous study [28]. To identify the key operational factors influencing the abundance of dominant genera (*Paracoccus* and *Pseudomonas*), we implemented an explainable machine learning framework. The analytical process integrated the following components: ☙ ensemble feature selection to screen robust predictors; & SVM modeling to capture complex, non-linear relationships; ● five-fold cross-validation to ensure model generalizability and mitigate overfitting; ❍ standard metrics (R^2 and RMSE) to evaluate predictive performance; and ■ SHAP analysis to quantify and interpret feature contributions. Further details are provided in Appendix A.

2.4 Pure culture denitrification experiment

Based on the meta-omics results, the dominant model species *Paracoccus pantotrophus* and *Pseudomonas aeruginosa,* which were present in the WWTP samples, were selected for pure-culture experiments to clarify the effect of different microbes and electron donors on denitrification performance (Fig. 1). *Paracoccus pantotrophus* (DSM2944) and *Pseudomonas aeruginosa* (CMCC10104) were obtained from the BeNa Culture Collection. Both strains were initially revived in peptone medium (10 $g \cdot L^{-1}$), and when the OD_{600} reached approximately 0.7–0.8, the cultures were harvested for use as denitrification inocula. Before inoculation, bacterial cells were collected by centrifugation at 10 000 $r \cdot min^{-1}$ for 10 min at 4 ℃, then washed three times with phosphate-buffered saline (PBS) to remove residual peptone medium and prevent interference from external electron donors. The washed cells were resuspended in PBS, and the suspension (0.5 mL) was inoculated into serum bottles, which were then supplied with H_2–CO_2, formate, and acetate separately. All the other experimental procedures were consistent with those described for the mixed-culture experiment.

The pure culture experiment was conducted in the sequential batch mode for three cycles. At the end of each cycle, samples were collected, and 15 mL of fresh growth medium was added to each reactor to maintain a constant working volume. Following the three batch cycles, all reactors were switched to a daily feeding regimen and operated for an additional 8 days to evaluate the stability of the denitrifying system.

2.5 EPS extraction and spectroscopic measurements

EPS was extracted using previously reported heating methods (Appendix A) [29,30]. Three distinct fractions were isolated, namely soluble EPS (S-EPS), loosely bound EPS (LB-EPS), and tightly bound EPS (TB-EPS). The three-dimensional excitation–emission matrix (EEM) spectra were obtained using an F-4700 spectrophotometer (HITACHI, Japan) equipped with a 1.0 cm quartz cell. The emission (EM) wavelengths ranged from 250–600 nm, and the excitation (EX) wavelengths ranged from 200–500 nm, both at 2 nm increments. The photomultiplier voltage was set to 700 V, and the excitation and emission slit widths were fixed at 5 nm. A scan speed of 30 000 $nm \cdot min^{-1}$ was employed, and Milli-Q water was used as the blank. Before EEM analysis, all samples were filtered through 0.45 μm membrane filters.

2.6 Analytical methods

The concentrations of nitrate (NO_3^--N) and nitrite (NO_2^--N) were quantified by ion chromatography (IC, Thermo Fisher Scientific , USA) using a Dionex™ InoPac™ AS11 analytical column (4 × 250 mm) and a protection column using 14 $mmol \cdot L^{-1}$ eluent (Dionex EGC 500 KOH, RFICTM Eluent Generator Cartridge; Thermo Fisher Scientific) for 15 min. Microbial growth was monitored by measuring the OD_{600} with a microplate reader (TENCAN Spark multimode; Thermo Fisher Scientific), which has been established as a reliable proxy for biomass concentration in liquid cultures [31]. N_2O concentration was analyzed using a gas chromatography system (Agilent 8890 GC, USA). Detailed procedures for analyzing PN, PS, TOC, and TN are provided in Appendix A.

3. Results and Discussion

3.1 Effects of electron donors on reactor performance in mixed culture

Batch tests were conducted to evaluate the impact of electron donors, such as H_2–CO_2, formate, and acetate, on

denitrification performance. Acetate-driven denitrification achieved the highest denitrification rate of 142.3 mg_N [illegible] was achieved within 24 h, accompanied by the highest biomass density (OD_{600}). However, this rapid nitrate reduction also resulted in the highest transient nitrite accumulation (35.97 $mg_N \cdot L^{-1}$), compared to approximately 15.04 $mg_N \cdot L^{-1}$ for formate and H_2 (Fig. 2(b)).

In contrast, formate and H_2 exhibited similar denitrification rates (51.6 and 48.3 $mg_N \cdot (L \cdot h \cdot OD_{600})^{-1}$, respectively). Formate, as a representative organic C1 electron donor, is less readily utilized in the TCA cycle for biomass synthesis [32]. This was reflected in its slower OD_{600} growth curve (Fig. 2(c)) and the lowest transcription levels of TCA cycle-related genes (6718.8 TPM), leading to an extended lag phase (approximately 24 h) before denitrification activity increased. In contrast, H_2 as a gaseous electron donor is limited by its low aqueous solubility (Henry's constant 1.279 $atm \cdot m^3 \cdot mol^{-1}$), which inherently restricts its microbial uptake and assimilation [20,33]. Nevertheless, H_2 offers the advantages of avoiding residual organic pollutants and producing less biomass (Fig. 2(c)), thereby improving process controllability [14].

Regarding sludge production, the EPS surrounding microbes is a major component of sludge, affecting its handling and disposal costs [12]. A detailed analysis of EPS, comprising PS and PN, revealed that its composition varied significantly among the electron donor groups. Acetate-driven denitrification was found to substantially stimulate PN secretion, particularly in the LB-EPS fraction, where the PN content was 2.4–2.9 fold greater than that of the other electron donors (Fig. 2(d)) [34]. In contrast, the PS content remained relatively consistent across conditions and represented the dominant EPS component (Fig. 2(e)) [35]. Consequently, the acetate-driven group exhibited the highest PN/PS ratio, which is known to enhance sludge flocculation and settleability [36–38]. These findings were further corroborated by fluorescence analysis using EEM spectroscopy (Fig. S3 in Appendix A).

Collectively, these results demonstrate that the choice of electron donor not only modulates denitrification kinetics and biomass yield but also directly shapes EPS compositions, thereby influencing critical sludge properties such as flocculation and settling in the mixed-culture experiment [39]. These insights are essential for optimizing electron donor selection in wastewater treatment to balance nitrogen-removal efficiency with sludge management requirements.

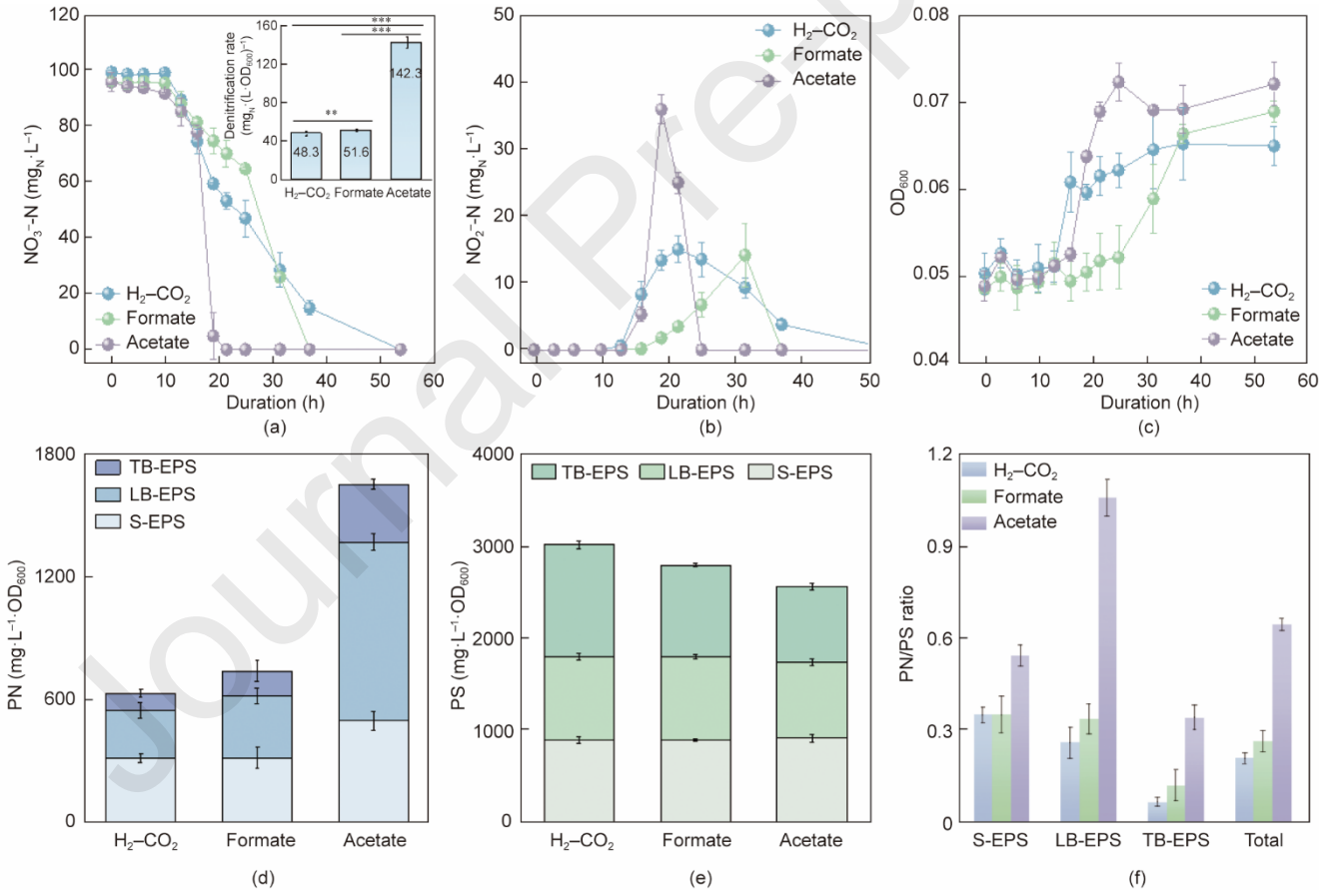

Fig. 2. Reactor performance and EPS composition with different electron donors. (a) The variation of nitrate concentration ($mg_N \cdot L^{-1}$) and denitrification rate ($mg_N \cdot (L \cdot h \cdot OD_{600})^{-1}$); (b) The variation of nitrite concentration ($mg_N \cdot L^{-1}$); (c) the variation in OD_{600}; (d) PN; (e) PS; and (f) PN/PS of different layers of EPS. Significance was determined using a two-tailed Student's *t*-test. A corrected *p*-value < 0.05 was considered significant. Asterisks represent significant differences at $*p < 0.05$, $**p < 0.01$, $***p < 0.001$).

3.2 Analysis of microbial community and dominant microbes in mixed culture

Bioprocess performance is strongly influenced by specific microorganisms, which are shaped by the available electron donors. Analysis of 16S rRNA sequencing data revealed the differences in alpha diversity across electron donor regimes. As presented in Table S3 in Appendix A, acetate-driven denitrification resulted in a noticeable decrease in richness (Chao index), evenness (Shannoneven index), and diversity (Shannon index), which is consistent with a recent study [17] and indicates the proliferation of certain functional microorganisms [4].

At the phylum level, Proteobacteria dominated across all experimental scenarios ((89.6% ± 7.6%); Fig. S4 in Appendix A), corroborating its widely reported prevalence in denitrification systems, particularly under acetate supplementation [4,40,41]. Notably, 41.8% of the MAGs were classified within this phylum (Fig. S1). Among the Proteobacteria, *Paracoccus* and *Pseudomonas* were identified as the primary denitrifying genera [42]. Both H_2- and formate-driven denitrification shared similar microbiota and were closely clustered in the hierarchical clustering tree analysis (Fig. S5 in Appendix A), with *Paracoccus* being dominant in both H_2-driven (59.3%) and formate-driven (68.3%) reactors (Fig. 3(a)), which is the most abundant in hydrogenotrophic denitrification reactors [43]. In comparison, *Pseudomonas* (88.4%) dominated in acetate-driven denitrification, with *Pseudomonas aeruginosa* (MAG23, 42.3%) and *Pseudomonas stutzeri* (MAG9, 39.1%) as the predominant species. Co-occurrence network analysis at the genus level further revealed that *Pseudomonas* occupied a central topological position in the acetate system, accounting for 3.9% of the total edges (Fig. S6 and Table S4 in Appendix A), suggesting its key role in maintaining community structure, possibly through the provision of public goods such as structural materials, signaling molecules, or enzymes [44,45].

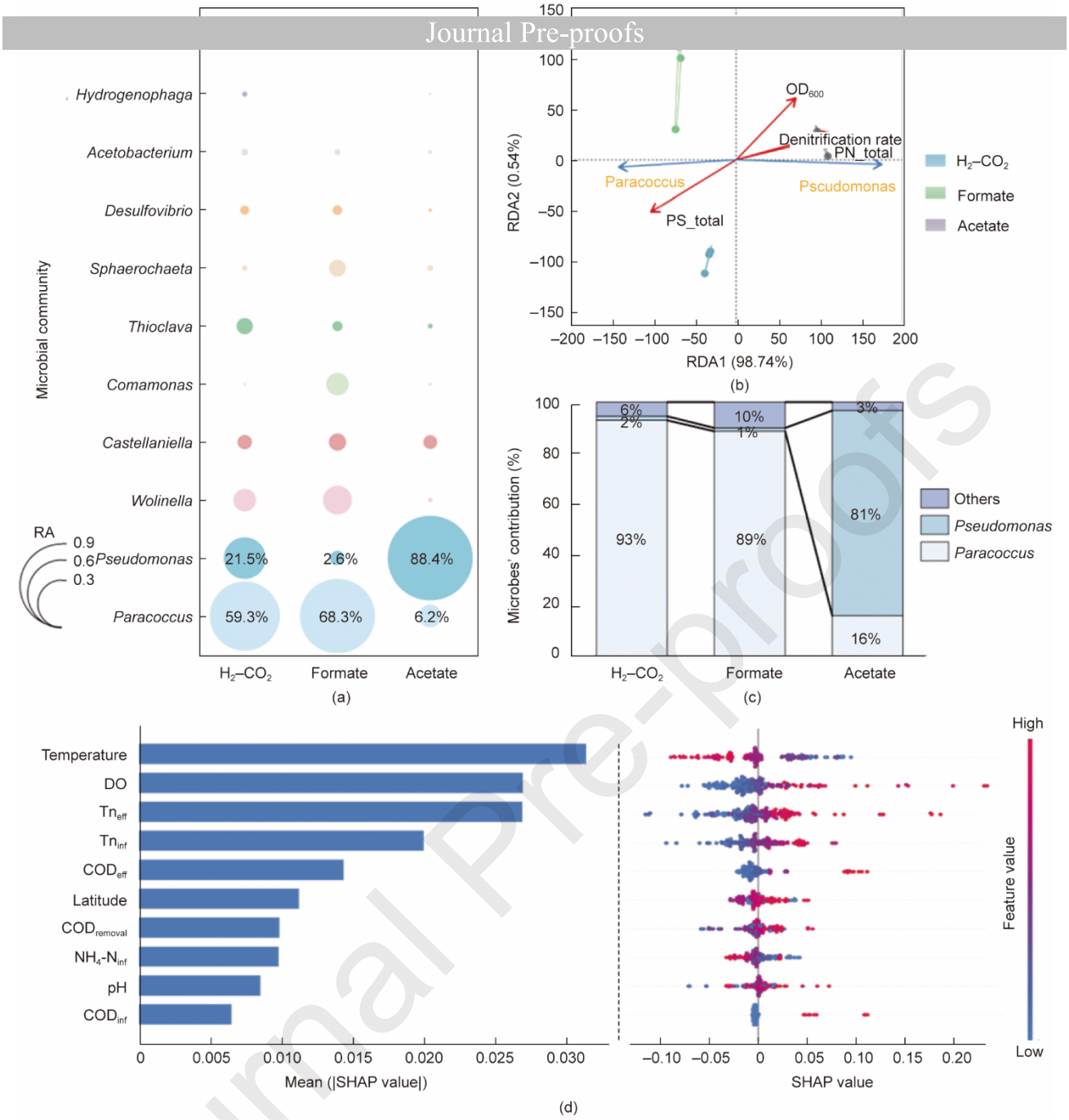

Fig. 3. Microbial responses to denitrification with different electron donors. (a) Microbial community shifting on the genus level under different electron donors based on 16S rRNA; (b) RDA of microbial community (top two at genus level) and critical reactor operation indicators for all scenarios (red and blue arrows represent operation indicators and microbes, respectively); (c) microbes' contribution to denitrification process; and (d) bar chart and swarm plot of SVMs result. The operational parameters (top 10) for *Pseudomonas* were analyzed using SVMs, and the impact of SHAP values on the model was examined (presented by the average and individual sample plots).

RDA explained 99.28% of the total variance at the genus level and clearly separated the three denitrification groups into distinct quadrants (Fig. 3(b)), underscoring the strong influence of electron donors on the microbial community structure. Samples of acetate-driven denitrification, genera (*Pseudomonas*), and reactor operation indicators (denitrification rate, nitrite content, and PN content) were clustered in the first quadrant, indicating strong positive relationships. *Pseudomonas* accounted for 81% of denitrification in the acetate-driven system (Fig. 3(c)). These relationships were further confirmed using Pearson's correlation analysis and Mantel's test (Fig. S7 in Appendix A). Specifically, the high denitrification rate and PN content were positively correlated with *Pseudomonas*, whereas OD_{600} was closely linked to both the acetate-driven group and the denitrification rate. In contrast, H_2- and formate-driven systems were located on the left side of the coordinate axis and showed a specific correlation with *Paracoccus*, which accounted for 89%-93% of denitrification in these systems (Fig. 3(c)).

Notably, both *Pseudomonas* and *Paracoccus* have been widely detected in full-scale WWTPs worldwide (Fig. S8 in Appendix A) [28]. *Pseudomonas* was detected in nearly all samples (> 99%) and generally had a higher relative abundance.

In contrast, *Paracoccus* was more likely to be detected in samples from Europe and Asia, with lower relative abundance. An SVM cing *Pseudomonas* abundance quantitatively. Comprehensive five-fold cross-validation revealed consistently strong model performance, with test set R^2 values ranging from 0.625 to 0.642 (mean = (0.637 ± 0.007)) and RMSE values between 1.281 and 1.296 (mean = (1.287 ± 0.007)) (Table S5 in Appendix A). The remarkably low standard deviations across folds underscore the model's stability, whereas the minimal training-testing performance gap (R^2 difference: 0.028) indicates effective overfitting prevention. SHAP analysis, which was applied to this robust model, quantitatively prioritized the influence of operational parameters on *Pseudomonas* abundance. The key drivers, ranked by their mean |SHAP value|, were temperature (SHAP ≈ 0.031), followed by DO (SHAP ≈ 0.027), and nitrogen concentrations, including both TN_{eff} (SHAP ≈ 0.027) and TN_{inf} (SHAP ≈ 0.021) (Fig. 3(d)). This indicates that temperature was the most influential factor, whereas the synergistic contributions of the nitrogen parameters reinforced the crucial role of *Pseudomonas* in the nitrogen-removal performance in full-scale WWTPs [46]. The widespread occurrence and high abundance of *Pseudomonas* in global WWTPs may reflect the common use of acetate as an electron donor. In contrast, *Paracoccus* showed no clear relationship with the analyzed operational parameters (Fig. S8 in Appendix A).

3.3 Mechanisms of reducing power generation through electron donor oxidation

3.3.1 H_2 as an electron donor

H_2 serves as a ubiquitous electron donor in natural and engineered environments and can diffuse directly into microbial cells [47,48]. Microbes utilize H_2 through metalloproteins called hydrogenases [48]. In our mixed-cultured experiment, multiple hydrogenases were expressed, among which *hyaA*, *hyaB*, *hyaC*, *hyaD*, and *hyaF* were significantly upregulated during H_2-driven denitrification compared to formate- and acetate-driven denitrification (Fig. 4(a)). Microbial contribution analysis revealed that the transcription of these hydrogenases was predominantly attributed to *Paracoccus pantotrophus* (MAG15, 73.3%–99.5%) in H_2-driven denitrification. Although both *Paracoccus pantotrophus* and *Pseudomonas aeruginosa* (MAG23) harbor hydrogenase genes (Fig. S9 in Appendix A) [48], the metabolic versatility and bioenergetic flexibility of *Paracoccus* [43] likely underlie the dominance of *Paracoccus pantotrophus* in the H_2-driven denitrification.

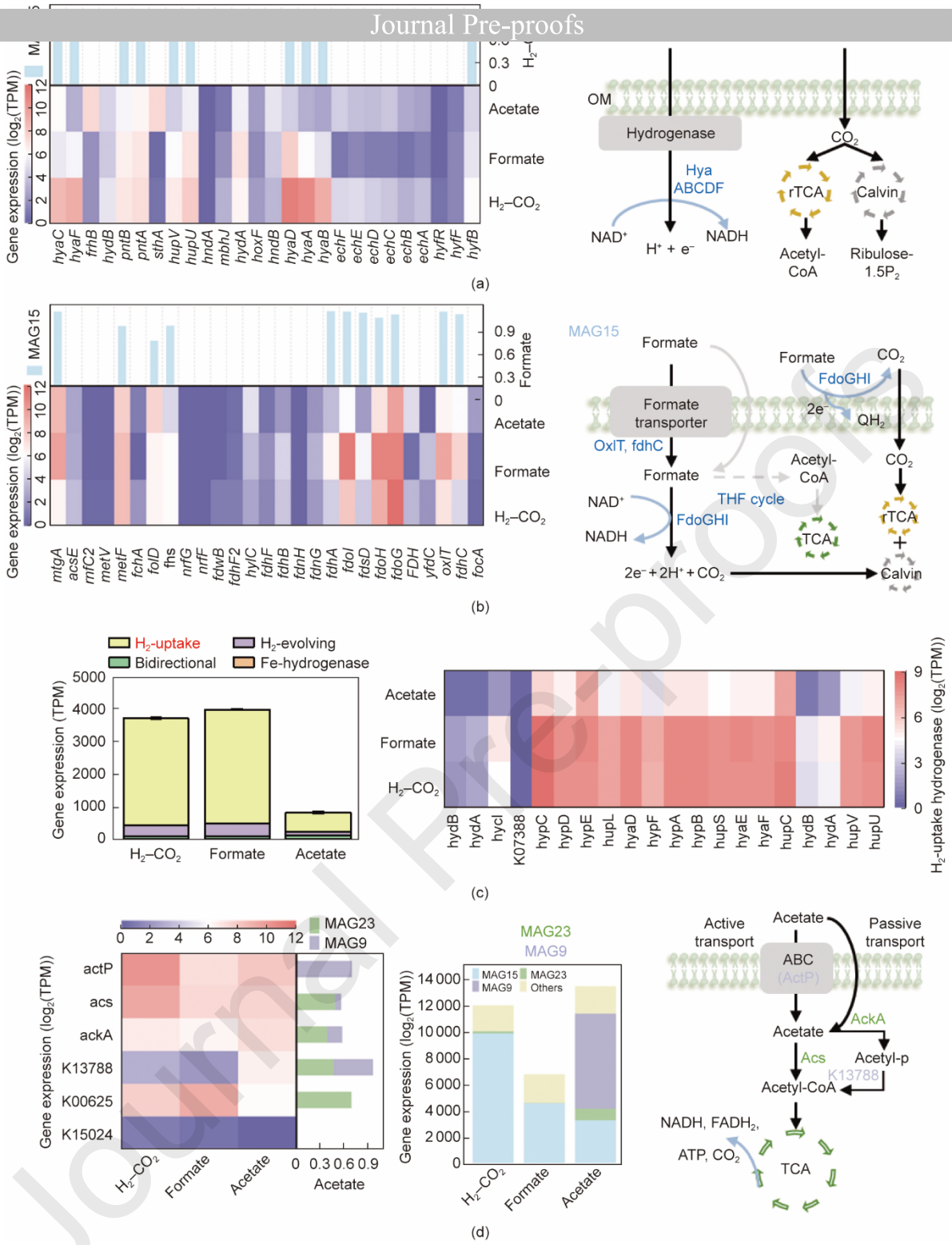

Fig. 4. Denitrification mechanisms of the different electron donors, heatmaps of genes, and the contribution by dominant species. (a) H_2 as an electron donor; (b) formate as an electron donor; (c) functional classification and gene transcription of hydrogenase (gene transcription was calculated based on $\log_2$(TPM); and (d) acetate as an electron donor; *Paracoccus pantotrophus* MAG15, *Pseudomonas aeruginosa* MAG23, *Pseudomonas stutzeri* MAG9).

H_2 oxidation by these enzymes yields low-potential electrons that are transduced through the respiratory chain for nitrate reduction, and CO_2 is indispensable in this process. CO_2 serves as an inorganic carbon source in the Calvin (M00165) and rTCA cycles (M00173; Fig. S10 in Appendix A) for biomass growth and regeneration [4,25]. Ribulose biphosphate carboxylase (RuBisCO, EC: 4.1.1.39) is the key enzyme in the Calvin cycle [49,50] and exhibited a significantly higher relative abundance (0.22%, $p < 0.001$) in H_2-driven denitrification (Fig. S11 in Appendix A), with *Paracoccus pantotrophus* contributing to 99.1% of its transcription. Notably, *Paracoccus pantotrophus* was the only species containing RuBisCo for

CO_2 fixation (Fig. S12 in Appendix A), leading to its dominance in H_2-driven denitrification (with CO_2 as the sole carbon sour[redacted]CA) supports its cellular metabolism and microbial regeneration in H_2-driven denitrification.

3.3.2 Formate as an electron donor

The transcription of formate transporters (*fdhC* and *oxIT*) was upregulated in formate-driven denitrification (Fig. 4(b)), implying that formate enters the cell primarily via active transport, a process predominantly mediated by *Paracoccus pantotrophus* (> 95.9%). Once inside the cell, formate can be metabolized via two pathways. One is the rapid conversion of formate into CO_2 via formate dehydrogenase, and the other is the conversion of formate into acetyl-CoA via the THF cycle (Fig. S13 in Appendix A). As shown in Fig. 4(b), the genes *fdoG*, *fdoH*, and *fdoI*, encoding key subunits of formate dehydrogenase, were abundant and significantly upregulated in formate-driven denitrification compared to denitrification by the other electron donors, with *Paracoccus pantotrophus* accounting for 91.2%–99.2% of their transcription. This upregulation suggests a metabolic preference for the direct oxidation of formate to CO_2, which is subsequently fixed via the Calvin or rTCA cycles. The initial metabolic pathways of H_2-driven and formate-driven denitrification were similar up to this point. NAD^+ is reduced to NADH, which can provide energy for cellular metabolic processes, such as denitrification [51]. Intriguingly, formate dehydrogenase is an H_2-evolving [NiFe]-hydrogenase [48] that is closely related to hydrogenase, leading to the development of similar microflora during H_2- and formate-driven denitrification. In addition, the transcription of H_2-uptake hydrogenases [52] was significantly upregulated in formate-driven denitrification (Fig. 4(c)), as in H_2-driven denitrification, further illustrating that they share a similar metabolism.

3.3.3 Acetate as an electron donor

Acetate is a widely used organic carbon source that enables rapid and complete denitrification [40]. It enters microbial cells via active or passive transport mechanisms (Fig. 4(d)) [53]. In acetate-driven denitrification, lower gene transcription of the acetate symporter (*actP*) is observed in *Pseudomonas stutzeri* (MAG9), suggesting that acetate crosses the membrane primarily by passive transport, without a specific uptake system, as previously reported [53]. Subsequently, intracellular acetate is converted to acetyl-CoA via the two pathways, AckA-K13788 and Acs. *Pseudomonas aeruginosa* preferentially uses the Acs pathway, whereas *Pseudomonas stutzeri* favors the AckA-K13788 pathway. Acetyl-CoA then enters the TCA cycle, as confirmed by the isotope experiment (Fig. S14 in Appendix A), generating NADH as the primary reducing power for denitrification. In acetate-driven denitrification, the transcriptional levels of TCA cycle genes were markedly higher than those of the other electron donors, supporting the synthesis of biomass precursors, production of reducing equivalents (NADH and $FADH_2$), and ATP generation [32].

3.4 The underlying denitrification metabolisms with different electron donors

Expectedly, denitrification was the dominant nitrogen metabolism pathway across all mixed-culture experiments with different electron donors (Fig. S15 in Appendix A). Electron transport via oxidative phosphorylation (accounted for 1.0%–1.4%) and flow direction determines stepwise nitrate reductions: $NO_3^- \rightarrow NO_2^- \rightarrow NO \rightarrow N_2O \rightarrow N_2$ (Fig. 5(a)). Generally, each step is catalyzed by specific enzymes such as membrane-bound nitrate reductase (Nar), periplasmic-bound nitrate reductase (Nap), nitrite reductase (Nir), nitric oxide reductase (Nor), and nitrous oxide reductase (Nos).

The initial reduction of nitrate to nitrite is mediated by either Nar or Nap. In this study, Nar was identified as the predominant enzyme (Fig. 5(b), Table S6 in Appendix A). Initially, NO_3^-/NO_2^- undergoes transmembrane transport through the nitrate/nitrite transporter (K02575), which is abundant in the H_2–CO_2 group and correlated with a high abundance of membrane-bound Nar. *Paracoccus pantotrophus* accounted for 96.6% of Nar transcription in H_2-driven denitrification. In contrast, *Pseudomonas stutzeri* preferentially catalyzed this step in the periplasm via Nap, accounting for 89.3%–93.6% of its transcription (Fig. 5(b)). The subsequent reduction of nitrite to nitric oxide, catalyzed by NirK or NirS, represents a central step in denitrification, as it marks the transition from dissolved to gaseous nitrogen species [54]. In this study, *nirS* was the dominant nitrite reductase gene, consistent with its widespread presence in Proteobacteria [55]. Nitric oxide (NO) is then converted into nitrous oxide (N_2O) by Nor, a membrane-bound cytochrome enzyme. The highest Nor abundance (0.36%) was observed in the acetate-driven denitrification reactors and was primarily expressed by *Pseudomonas stutzeri* and *Pseudomonas aeruginosa*. In *Pseudomonas aeruginosa*, Nor not only supports anaerobic respiration but also serves as a detoxifier against exogenous NO [56], contributing 44.4%–46.8% of total Nor transcription. Finally, N_2O is reduced to N_2 by Nos, a Cu-containing enzyme located in the periplasm, which was also abundant in acetate-driven reactors (0.32%). The Nor genes were more abundant than the Nos genes in the acetate-driven reactor, with a Nor/Nos ratio of 1.09, compared to 0.62 and 0.60 for H_2- and formate-driven denitrification, respectively. The production/consumption ratio can be a genetic indicator to predict the net production of intermediates, such as N_2O [57], which is consistent with the pure culture results, where acetate-driven denitrification had the highest N_2O concentration (8.6 ppm) at the beginning. However, the higher abundance of Nos in the acerate-driven group drastically decreased to 0.5 ppm. Although *Paracoccus pantotrophus*, *Pseudomonas aeruginosa,* and *Pseudomonas stutzeri* all harbor complete denitrification genes, their relative contributions to each reduction

step differ significantly, suggesting a potential division of labor that may optimize metabolic resource allocation [55].

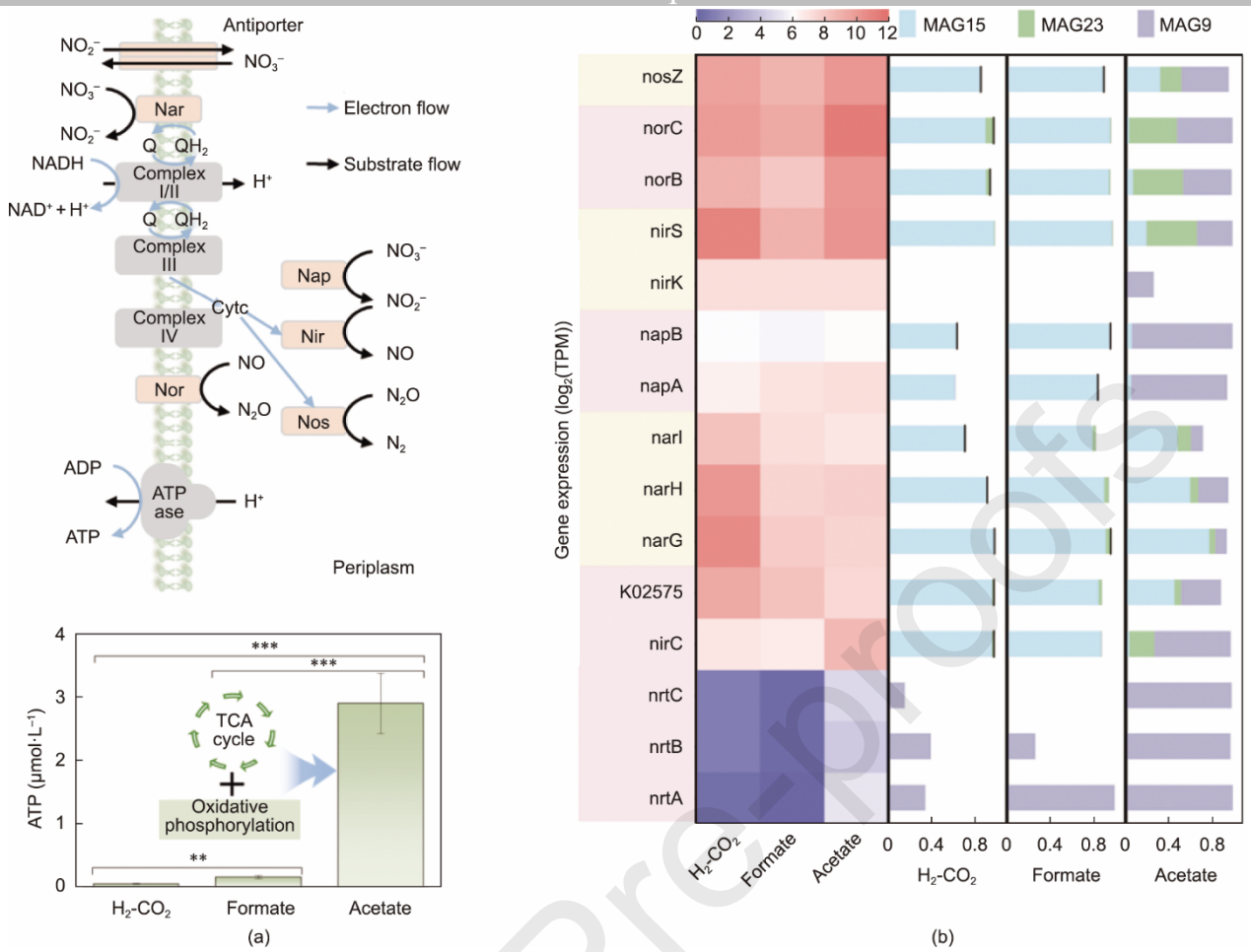

Fig. 5. Denitrification process with different electron donors. (a) The metabolic process of denitrification; (b) heatmap of genes and the contribution by dominant species (gene transcription was calculated based on $\log_2$(TPM); *Paracoccus pantotrophus* MAG15, *Pseudomonas aeruginosa* MAG23, *Pseudomonas stutzeri* MAG9.

During denitrification, microbial oxidation of electron donors generates substantial amounts of NADH, and the subsequent reduction of ubiquinone contributes to the proton motive force that powers ATP synthesis [58]. Specifically, acetate oxidation via the TCA cycle yields significant amounts of NADH and ATP, theoretically producing approximately 5.2 ATP per mol of acetate consumed [59]. In comparison, H_2 and formate are oxidized at the outer layer of the cytoplasmic membrane, transferring electrons directly to quinones (Q/QH_2), a pathway that supports lower ATP synthesis [59,60]. The higher redox potential of the NAD^+/NADH couple (219.2 kJ·mol^{-1}) compared to that of the quinone pool (150 kJ·mol^{-1}) enables more efficient electron transfer and enhanced ATP production via oxidative phosphorylation. ATP is the energy carrier for denitrification [61] and is generated mainly by the F-type ATPase (M00157) present in bacteria (Table S7 in Appendix A) [62]. In this study, acetate-driven denitrification yielded the highest ATP content, 51 and 18 fold higher than that of H_2- and formate-driven denitrification, respectively (Fig. 5(a)), which was consistent with the metatranscriptome results (2-fold higher than those of H_2- and formate-driven denitrification).

In summary, in H_2- and formate-driven denitrification, *Paracoccus pantotrophus* performs the complete denitrification pathway by coupling the oxidation of the electron donor with the reduction of nitrate to N_2. Complete denitrification can maximize energy generation [55], which is more likely to occur in systems where energy is more difficult to obtain (lower ATP). In contrast, acetate-driven denitrification systems exhibit a cooperative mode of denitrification, with differentiated contributions from *Paracoccus pantotrophus*, *Pseudomonas aeruginosa*, and *Pseudomonas stutzeri* in distinct enzymatic steps, reflecting a distinct metabolic division of labor.

3.5 Biomass growth and EPS production

Microbial biomass is primarily attributed to cellular replication, accompanied by the secretion of EPS to enhance survival in harsh environments (Fig. 6(a)), which are the main components of sludge [63,64]. DNA replication is the core cellular replication pathway. Transcription of the DNA replication gene correlated well with the OD_{600} (Fig. 2(c)) across the different electron donors. *Paracoccus pantotrophus,* as the core species, mainly contributed to DNA replication during denitrification

driven by H_2 (73.8%) and formate (78.3%). In acetate-driven denitrification, *Pseudomonas aeruginosa* was the dominant specDNA replication was demonstrated in the pure culture experiment, in which *Pseudomonas aeruginosa* maintained a stable biomass level across all electron donors (0.27–0.29 mg·mL^{-1}; Table S8, Fig. S16 in Appendix A).

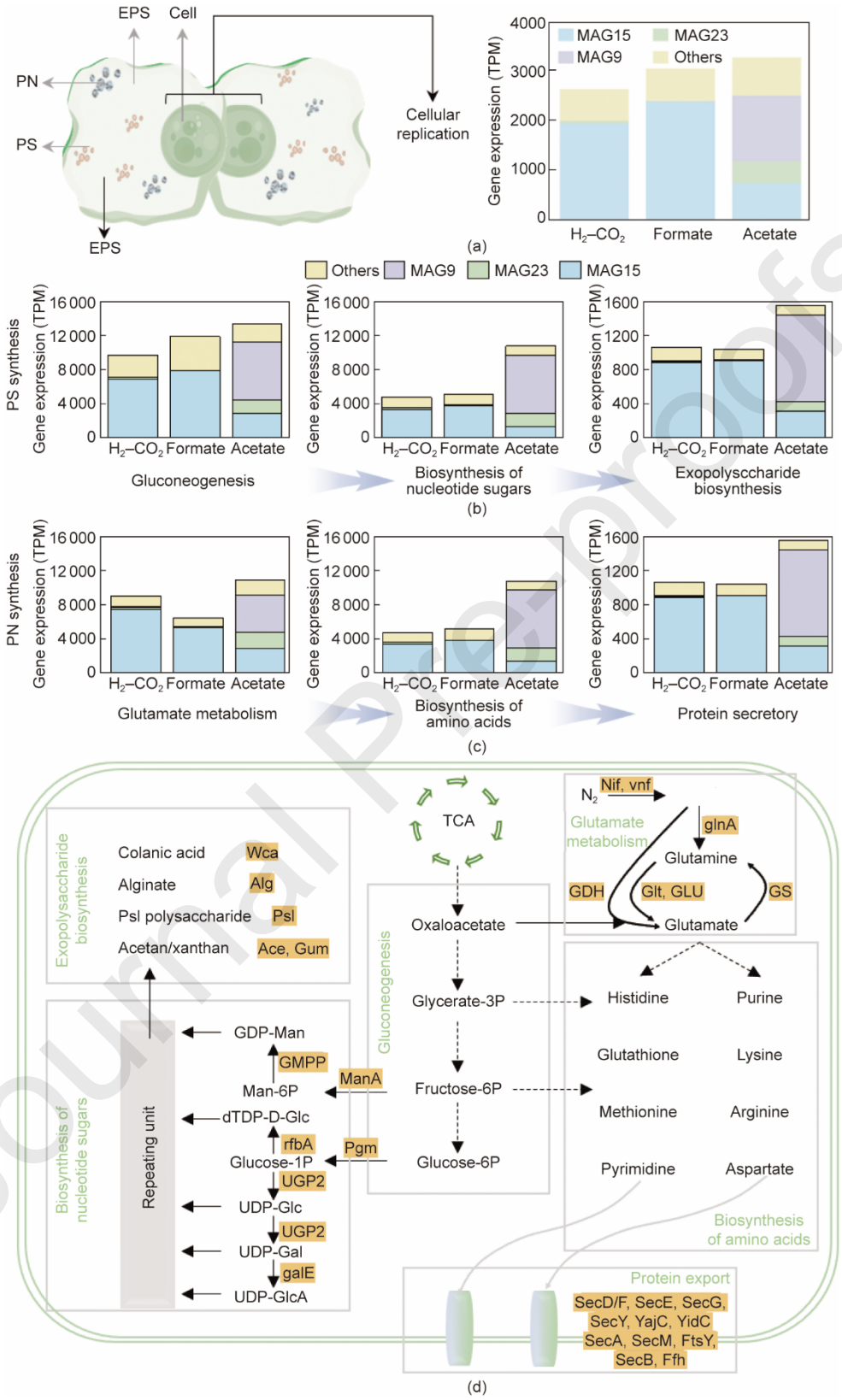

Fig. 6. EPS and biomass biosynthesis pathways. (a) The structure of microbial EPS and the transcription of DNA replication; (b, c) the gene transcription of key processes of (b) PS and (c) PN synthesis; and (d) the metabolism pathway of EPS generation.

In addition to DNA replication, *Pseudomonas aeruginosa* also showed negligible involvement in PS (Fig. 6(b)) and PN synt[Journal Pre-proofs]cess, involving three main steps in both PS and PN biosynthesis (Fig. 6(d)). The transcription of PN biosynthesis (Fig. 6(b)) was consistent with the actual PN content (Fig. 2(d)) during denitrification, with the acetate-driven system exhibiting the highest transcription. Differences in PS content and gene transcription may be due to the translation process. The lower contribution of *Pseudomonas aeruginosa* to EPS formation is associated with reduced pyocyanin production under anaerobic conditions, which is essential for EPS and biofilm formation [56]. In H_2- and formate-driven reactors, *Paracoccus pantotrophus* was the primary contributor to almost all metabolic pathways (Figs. 6(b) and (c)).

In summary, *Paracoccus pantotrophus*, the dominant species in H_2- and formate-driven denitrification, mainly contributed to cellular replication and EPS formation. In contrast, *Pseudomonas aeruginosa*, although dominant in acetate-driven denitrification, only contributed 10%–20% to biomass and EPS biosynthesis. *Pseudomonas stutzeri* contributed to the large amount of sludge and biomass generated in the acetate-driven mix-culture denitrification.

3.6 Pure culture investigation

Based on the meta-omics results, two dominant and model denitrifiers, *Paracoccus pantotrophus* and *Pseudomonas aeruginosa,* were selected to investigate the effects of different electron donors on denitrification performance. Successive acclimation cycles markedly enhanced the denitrification rates of both species, although distinct differences were observed (Fig. 7(a)). In all three cycles, acetate-driven denitrification consistently achieved outstanding performance, similar to that observed in the mixed-culture experiments, with denitrification rates increasing by approximately 2.4–3.4 fold. Notably, *Pseudomonas aeruginosa* outperformed *Paracoccus pantotrophus* under acetate-driven scenarios by 1.6–2.4 fold. In H_2- and formate-driven systems, *Paracoccus pantotrophus* exhibited slightly higher denitrification rates than *Pseudomonas aeruginosa*. This divergence aligns with the mixed cultures, suggesting that acetate is particularly effective when paired with specific denitrifiers.

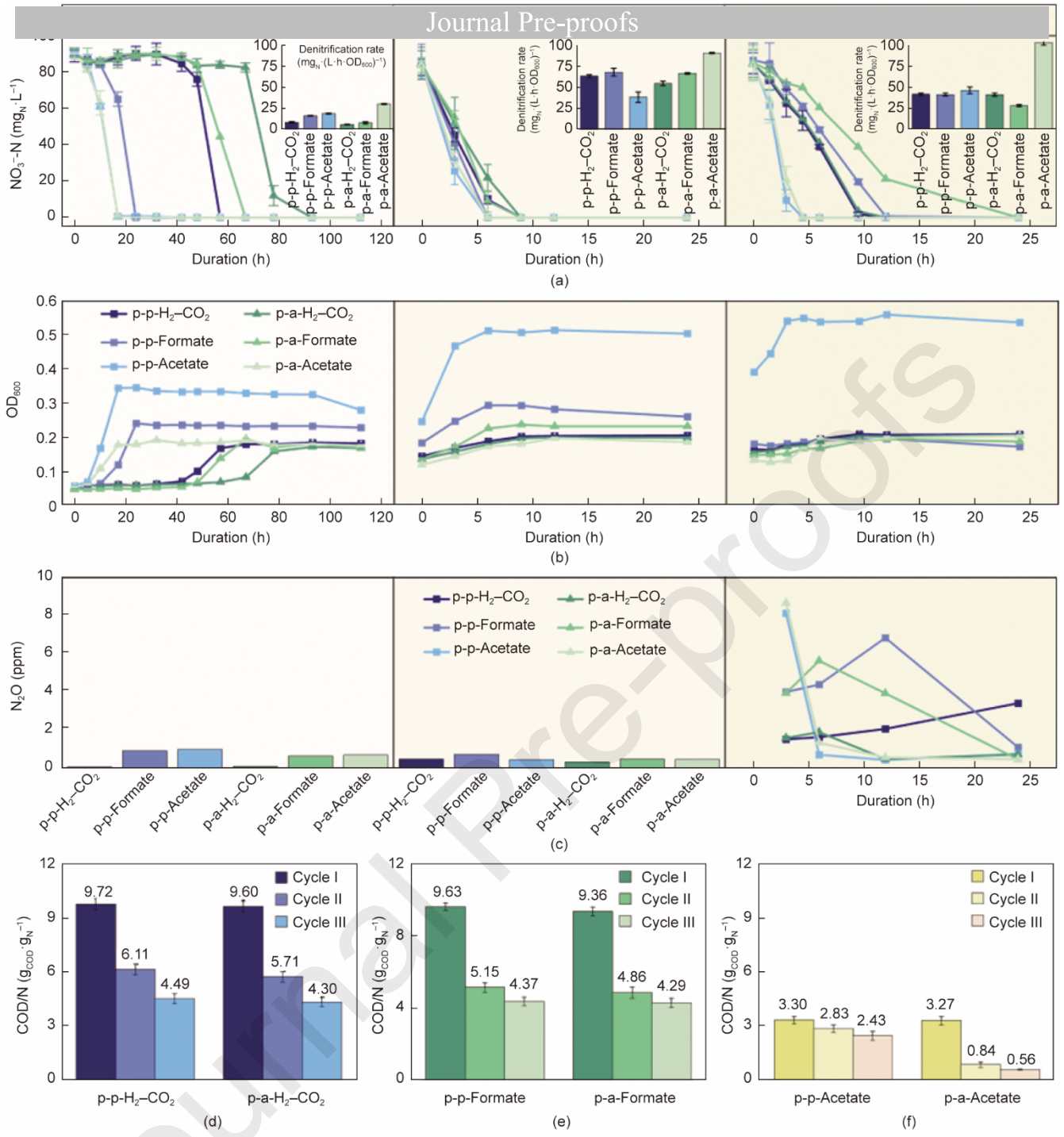

Fig. 7. Denitrification performance of domain pure cultures. (a) Nitrate concentration ($mg_N \cdot L^{-1}$) curve and denitrification rate ($mg_N \cdot (L \cdot h \cdot OD_{600})^{-1}$) of two pure cultures with different electron donors; (b) OD_{600} curve; (c) N_2O concentration (in cycle I&II N_2O test at the end of cycle, in cycle III gas samples were analyzed at 3, 6, 12, and 24 h); and the COD/N levels ($g_{COD} \cdot g_N^{-1}$) in the (d) H_2-CO_2-fed, (e) formate-fed, and (f) acetate-fed scenarios. p.p, *Paracoccus pantotrophus*; p.a, *Pseudomonas aeruginosa*.

As the denitrification process proceeded, the biomass yield (OD_{600}) exhibited a species-dependent behavior (Fig. 7(b)). For *Paracoccus pantotrophus*, acetate supported the highest biomass, followed by formate and H_2–CO_2, indicating that acetate promoted vigorous cell growth. In contrast, *Pseudomonas aeruginosa* maintained a stable biomass level across all electron donors, and is prone to slow growth and generates less biomass under anaerobic environments [56]. Remarkably, with acetate as the electron donor, *Pseudomonas aeruginosa* not only sustains a high denitrification rate (103.8 compared to 46.9 $mg_N \cdot (L \cdot h \cdot OD_{600})^{-1}$ for *Paracoccus pantotrophus*) but also limits biomass production (OD_{600} 0.20 vs 0.54). This combination underscores a promising bioaugmentation strategy: deploying *Pseudomonas aeruginosa* with acetate effectively reduces sludge production while maintaining robust nitrate removal. Similarly, a previous study selected *Pseudomonas aeruginosa* as a bioaugmentation strategy to recruit high-efficiency denitrifying consortia for wastewater with high nitrate content [44]. Overall, these results underscore that both electron donor type and microbial identity are key determinants of sludge

production [20,40].

R[illegible]54]. In cycles I&II, the gas samples were analyzed only at the end. Thus, N_2O was almost completely reduced to N_2, resulting in a low concentration (Fig. 7(c)). In cycle III, gas samples were collected at four sampling points to determine the N_2O concentrations as denitrification progressed. Faster denitrification (as in the acetate-driven systems) led to an earlier N_2O peak. The highest N_2O concentration (8.6 ppm) was observed in the acetate-driven reactor, but it decreased rapidly to 0.5 ppm regardless of the denitrifiers, indicating that sufficient reaction time is necessary to minimize N_2O emissions in acetate-based denitrification.

Intriguingly, as the reaction proceeded and acclimation took effect, the overall requirement for electron donors decreased, as indicated by the declining COD/N ratio (Figs. 7(d)–(f)), and biomass levels stabilized [9]. The COD/N ratio was the lowest in acetate-driven reactors, with *Pseudomonas aeruginosa* consuming significantly less acetate (0.56 $g_{COD} \cdot g_N^{-1}$ in cycle III) than *Paracoccus pantotrophus* (2.43 $g_{COD} \cdot g_N^{-1}$). The biomass yield is closely related to the electron donor utilized for cell synthesis (f_s), a critical parameter in denitrification [21], which explains why *Pseudomonas aeruginosa* obtained a lower biomass yield (Fig. 7(b)). As a facultative bacterium, the denitrification of *Pseudomonas aeruginosa* can be regulated by the transcriptional regulators ANR, DNR, and NarXL, which significantly decrease biomass biosynthesis when conditions shift from aerobic to anaerobic [65,66].

Meta-omics analyses further revealed that *Pseudomonas aeruginosa* contributed less to the top three pathways under acetate conditions (13.1% for energy metabolism, 19.5% for amino acid metabolism, and 14.7% for membrane transport), resulting in lower electron donor utilization and restrained biomass synthesis. Thus, pairing *Pseudomonas aeruginosa* with acetate sustains high denitrification efficiency while generating less biomass, underscoring its potential for practical nitrate removal in wastewater treatment. This approach promises to reduce sludge-handling costs and improve process controllability, making it an attractive strategy for sustainable denitrification.

3.7 Economic, ecological, and engineering implications analysis

The proper selection of electron donors for denitrification should be based on several criteria. While previous studies have focused more on the cost of electron donors, specific substrate utilization (SSU), biomass yield (BY), and denitrification rate (DR) [20,49]. The pursuit of carbon neutrality highlights the role of WWTPs as significant sources of GHG emissions [13]. For instance, the A2O technology has been reported to emit 6.19 $g_{N_2O} \cdot kg_{TN}^{-1}$ influent and 375.53 $g_{CO_2} \cdot kg_{COD}^{-1}$ [67]. This study further evaluated the electron donors with regard to carbon emissions (CO_2E), N_2O emissions (N_2OE), toxicity, and transportability (Fig. 8).

From an economic perspective, H_2 is the most favorable option. H_2 is the cleanest and cheapest (0.02 $USD \cdot mol_{nitrate}^{-1}$) electron donor for denitrification, and hydrogenotrophic denitrifiers entail the lowest disposal costs due to their minimal biomass yield in mixed cultures (0.23 $g_{cell} \cdot g_{nitrate}^{-1}$) [20] (Table S9). Moreover, H_2-driven denitrification is a CO_2-sequestration process that achieves negative CO_2 emissions (–0.138 $mol_{CO_2} \cdot mol_{nitrate}^{-1}$) by fixing CO_2 into biomass. However, a major limitation of H_2 is its relatively low denitrification rate (48.3 $mg_N \cdot (L \cdot h \cdot OD_{600})^{-1}$; Fig. 2(a)), which stems from constraints on gas–liquid mass transfer [20, 33]. Additional challenges include difficulties with H_2 storage and transportation, which carry the risk of leakage and spontaneous combustion due to the vulnerability of the material [68].

Although formate exhibits high solubility in water and polar solvents, which facilitates its storage and transport [23,69], it does not stand out in terms of denitrification rate, CO_2 emissions, or N_2O emissions. Another drawback of using formate is its toxicity, as reflected by the lowest live/dead cell ratio observed in all scenarios (0.68–0.70; Fig. S17 in Appendix A). Formate toxicity is attributed to the inhibition of respiratory cytochromes and may be exacerbated by the diffusion of the protonated acids across the cell membrane, which acidifies the cytoplasm and reduces the proton motive forces [70]. Furthermore, the addition of formate increases the pH (> 8.5) of the system (Fig. S18 in Appendix A); therefore, formate is not recommended for long-term operation.

From the perspective of treatment efficiency, acetate was the optimal choice. It required the lowest dosage to reduce a given amount of nitrate, as indicated by its minimal SSU (Fig. 7(b)). Acetate has an excellent denitrification rate (142.3 $mg_N \cdot (L \cdot h \cdot OD_{600})^{-1}$) compared to nearly all other inorganic and organic donors [20,40]. The types of microbes also affect the denitrification efficiency, as *Pseudomonas aeruginosa* has a higher denitrification rate than *Paracoccus pantotrophus* in an acetate-fed system. In addition, combining acetate with the bioaugmenting denitrifying bacterium *Pseudomonas aeruginosa* can significantly reduce sludge yield and provide sufficient reaction time (6 h), helping mitigate N_2O emissions (Fig. 7(c)). The higher PN/PS of the EPS makes it easier to dispose of the sludge. Presumably, the on-site acetate generation via the WLP could enable green, efficient, and sustainable denitrification, with low CO_2 emissions (fixed by the sidestream acetate from the WLP; Fig. 8(a)) and minimized sludge yield (mediated by *Pseudomonas aeruginosa*; Fig. 7(b)).

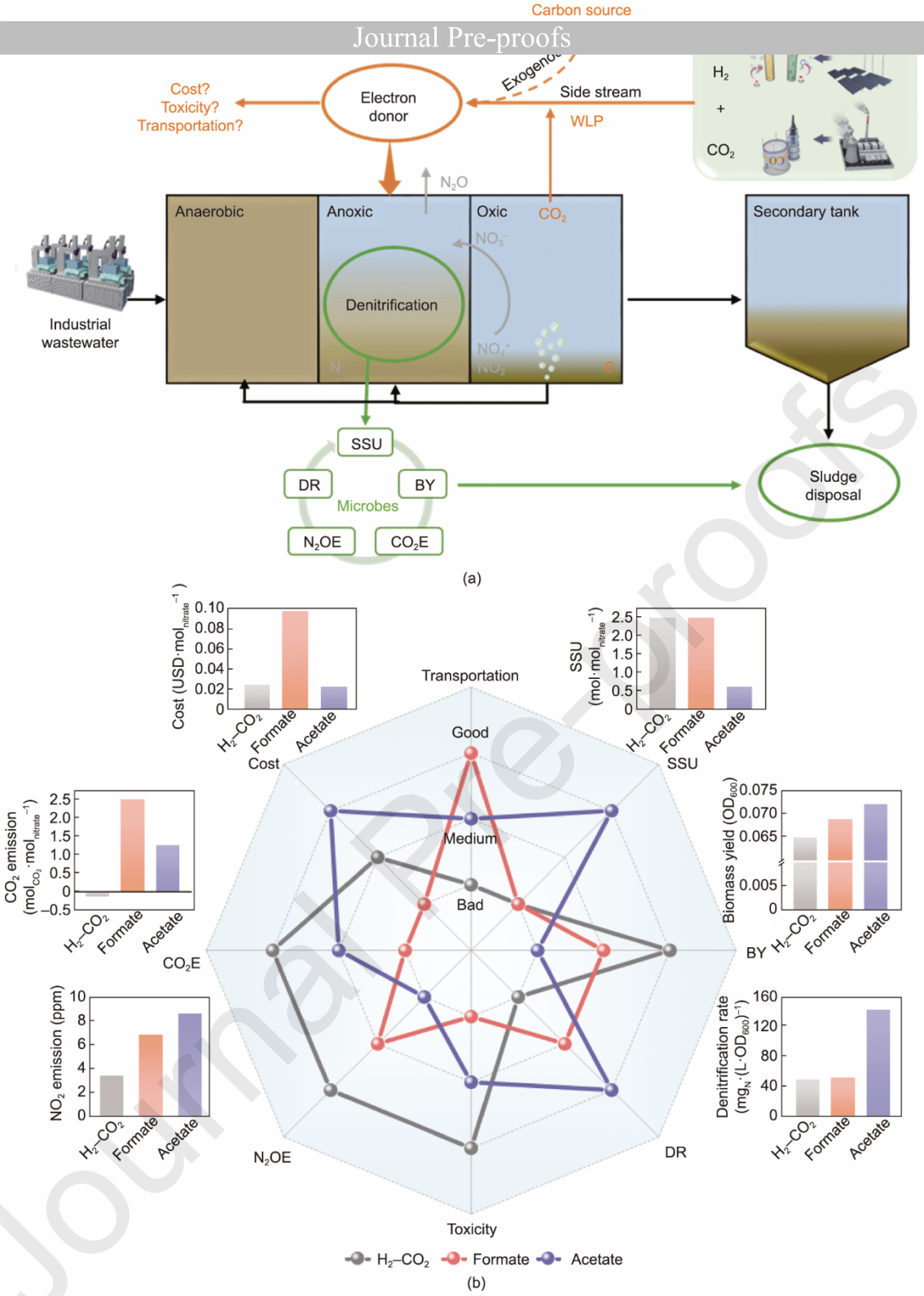

Fig. 8. The comparison of different electron donors in denitrification. (a) The denitrification process in wastewater treatment plants and (b) a comparison of different electron donors considering several factors, SSU: specific substrate utilization; BY: biomass yield; DR: denitrification rate; CO_2E: carbon emission; N_2OE: N_2O emission. The innermost and outermost parts of the octagon represent the lowest and highest scores (bad and good, respectively), respectively. The original data are presented in Table S9 in Appendix A.

4. Conclusions

High-performance denitrification is pivotal in WWTPs, where the selection of optimal electron donors and microbial communities is critical. The proper selection of electron donors substantially influences the microbial composition. Notably, H_2 and formate as electron donors fostered similar microbial communities and metabolic pathways, with *Paracoccus* being the dominant genus and *Paracoccus pantotrophus* being the predominant species. In contrast, acetate-driven denitrification

was primarily associated with *Pseudomonas*, a genus frequently observed in WWTP microbial samples worldwide ($n = 1186$), and [redacted] tate-driven denitrification, stands out as an energy-efficient microbe characterized by reduced electron donor consumption and minimal biomass production while maintaining the highest denitrification rate. These findings provide a framework for achieving a low-emission denitrification process using a bioaugmentation dosage (*Pseudomonas aeruginosa*) and a selective electron donor (acetate) for enhanced denitrification performance. Furthermore, integrating on-site acetate production via the WLP as a sidestream process offers a promising route to reduce operational costs and the overall carbon footprint.

Abbreviations

WWTPs: wastewater treatment plants; SVMs: support vector machine; rRNA: ribosomal RNA; R^2: coefficient of determination; RMSE: root mean square error; SHAP: Shapley Additive exPlanations; EPS: extracellular polymeric substances; TOC: total organic carbon; TN: total nitrogen; PN: protein; DO: dissolved oxygen; PS: polysaccharides; TCA: tricarboxylic acid; rTCA: reductive TCA; PCoA: principal coordinate analysis; RDA: redundancy analysis; NADH: Nicotinamide adenine dinucleotide; $FADH_2$: Flavine adenine dinucleotide, reduced; ATP: adenosine triphosphate; THF: tetrahydrofolate; TPM: transcripts per million; FDH: formate dehydrogenase; RuBisCO: ribulose biphosphate carboxylase; Nar: membrane-bound nitrate reductase; Nap: periplasmic-bound nitrate reductase: Nir: nitrite reductase; Nor: nitric oxide reductase; Nos: nitrous oxide reductase; A2O: anaerobic/anoxic/oxic; SSU: specific substrate utilization; BY: biomass yield; DR: denitrification rate; CO_2E: carbon emission; N_2OE: N_2O emission; COD: chemical oxygen demand; WLP: Wood-Ljungdahl pathway; OD_{600}: biomass density; ANR: anaerobic regulation of arginine deiminase and nitrate reduction; DNR: dissimilative nitrate respiration regulator; NarXL: two-component nitrate-sensing system; CO_2 emission for treating per cubic meter of wastewater: $gCO_2eq \cdot m^{-3}$; denitrification rate: $mg_N \cdot (L \cdot h \cdot OD_{600})^{-1}$; the consumption of COD per nitrate: $g_{COD} \cdot g_N^{-1}$; N_2O emission per total nitrogen: $g_{N_2O} \cdot kg_{TN}^{-1}$; CO_2 emission per COD: $g_{CO_2} \cdot kg_{COD}^{-1}$; cost for treating mol of nitrate: $USD \cdot mol_{nitrate}^{-1}$; biomass generation for treating nitrate: $g_{cell} \cdot g_{nitrate}^{-1}$; CO_2 emission for treating mol of nitrate: $mol_{CO_2} \cdot mol_{nitrate}^{-1}$; TN_{eff}: total nitrogen in effluent; TN_{inf}: total nitrogen in influent; COD_{eff}: COD in effluent; COD_{inf}: COD in influent; $COD_{removal}$: the removal of COD; $NH_4\text{-}N_{inf}$: NH_4-N in influent.

Author information

Jing Zhao conceived the idea and performed experiments for this work. Yunjie Liao performed the modeling analysis. Jing Zhao and Yuting Wang performed the samples and data analysis. Jing Zhao contributed to the writing and revision of the manuscript. RuiPing Liu contributed to the revision of the manuscript. Qinghua Ji, RuiPing Liu, and HuiJuan Liu supervised the research.

Data availability

Data will be made available on request.

Acknowledgments

This work was supported by the National Natural Science Foundation of China (52192683, 52200165, and 52221004), the Postdoctoral Research Foundation of China (2023M731935 and YJ20220129), and the Beijing Outstanding Young Scientist Program (JWZQ20240101005).

References

[1] Jiang M, Zheng J, Perez-Calleja P, Picioreanu C, Lin H, Zhang X, et al. New insight into CO2-mediated denitrification process in H2-based membrane biofilm reactor: an experimental and modeling study. Water Res 2020;184:116177.

[2] Rahimi S, Modin O, Mijakovic I. Technologies for biological removal and recovery of nitrogen from wastewater. Biotechnol Adv 2020;43:107570.

[3] Ma B, Yang W, Li N, Kosolapov DB, Liu X, Pan S, et al. Aerobic denitrification promoting by actinomycetes coculture: investigating performance, carbon source metabolic characteristic, and raw water restoration. Environ Sci Technol 2024;58(1):683–94.

[4] Wang P, Wu Y, Yang L, Zheng X, Long M, Chen Y. Inorganic carbon metabolism enhanced hydrogen-driven denitrification: evaluation of carbon fixation pathways and microbial traits. Chem Eng J 2024;497:154528.

[5] Liu YL, Zhang WY, Chen W. Denitrification technology and the catalysts: a review and recent advances. ChemCatChem 2024;16(15):e202301662.

[6] Huang S, Fu Y, Zhang H, Wang C, Zou C, Lu Y. Research progress of novel bio-denitrification technology in deep wastewater treatment. Front Microbiol 2023;14:1284369.

[7] Zhang XX, et al. Improvement of biological nitrogen removal with nitrate-dependent Fe(II) oxidation bacterium B6 in an up-flow bioreactor for wastewater treatment. Bioresour Technol 2016;219:624–31.

[8] Chen YZ, Zhang LJ, Ding LY, Zhang YY, Wang XS, Qiao XJ, et al. Sustainable treatment of nitrate-containing wastewater by an autotrophic hydrogen-oxidizing bacterium. Environ Sci Ecotechnol 2022;9:100146.

[9] Pan Y, Hua TW, Sun RZ, Fu YY, Xiao ZC, Wang J, et al. Machine learning-assisted optimization of mixed carbon source compositions for high-performance denitrification. Environ Sci Technol 2024;58(28):12498–508.

[10] Tian T, Yu HQ. Denitrification with non-organic electron donor for treating low C/N ratio wastewaters. Bioresour Technol 2020;299:122686.

[11] Fu X, Hou R, Yang P, Qian S, Feng Z, Chen Z, et al. Application of external carbon source in heterotrophic denitrification of domestic sewage: a review. Sci Total Environ 2022;817:153061.

[12] Murray A, Horvath A, Nelson KL. Hybrid life-cycle environmental and cost inventory of sewage sludge treatment and end-use scenarios: a case study from China. Environ Sci Technol 2008;42(9):3163–9.

[13] Song C, Zhu JJ, Yuan Z, van Loosdrecht MCM, Ren ZJ. Defining and achieving net-zero emissions in the wastewater sector. Nat Water 2024;2(10):927–35.

[14] Li R, Lu M, Guo R, Duan H, Ni B, Fu S. Life cycle assessment of hydrogenotrophic denitrification in membrane aerated biofilm reactors for sustainable wastewater treatment. Water Res 2024;267:122529.

[15] Wu J, Yin Y, Wang J. Hydrogen-based membrane biofilm reactors for nitrate removal from water and wastewater. Int J Hydrogen Energy 2018;43(1):1–15.

[16] Carlson HK, Lui LM, Price MN, Kazakov AE, Carr AV, Kuehl JV, et al. Selective carbon sources influence the end products of microbial nitrate respiration. ISME J 2020;14(8):2034–45.

[17] Pan Y, Sun RZ, Wang Y, Chen GL, Fu YY, Yu HQ. Carbon source shaped microbial ecology, metabolism and performance in denitrification systems. Water Res 2023;243:120330.

[18] Blohm A, Kumar S, Knebl A, Herrmann M, Küsel K, Popp J, et al. Activity and electron donor preference of two denitrifying bacterial strains identified by Raman gas spectroscopy. Anal Bioanal Chem 2022;414(1):601–11.

[19] Yang J, Qin Y, Liu X, Yang L, Zheng S, Gong S, et al. Effects of different electron donors on nitrogen removal performance and microbial community of denitrification system. J Environ Chem Eng 2022;10(3):107915.

[20] Di Capua F, Pirozzi F, Lens PNL, Esposito G. Electron donors for autotrophic denitrification. Chem Eng J 2019;362:922–37.

[21] Guo JS, Fang F, Yan P, Chen YP. Sludge reduction based on microbial metabolism for sustainable wastewater treatment. Bioresour Technol 2020;297:122506.

[22] Huang Y, Igarashi K, Liu L, Mayumi D, Ujiie T, Fu L, et al. Methanol transfer supports metabolic syntrophy between bacteria and archaea. Nature 2025;639(8053):190–5.

[23] Zhang J, Guo L, Gao C, Song W, Wu J, Liu L, et al. Metabolic engineering strategies for microbial utilization of C1 feedstocks. Syst Microbiol Biomanuf 2023;3(1):122–36.

[24] Salazar G, Paoli L, Alberti A, Huerta-Cepas J, Ruscheweyh HJ, Cuenca M, et al. Gene expression changes and community turnover differentially shape the global ocean metatranscriptome. Cell 2019;179(5):1068–83.e21.

[25] Li Y, Wang Y, Dong F, Yuan S, Hu Z, Wang W. Controlling carbon dioxide-to-hydrogen ratio to improve hydrogen utilization and denitrification rates of hydrogenotrophic autotrophic denitrification through homoacetogenesis-heterotrophic denitrification pathway. Bioresour Technol 2024;393:130116.

[26] Ni M, Pan Y, Li D, Huang Y, Chen Z, Li L, et al. Metagenomics, metatranscriptomics, and proteomics reveal the metabolic mechanism of biofilm sequencing batch reactor with higher phosphate enrichment capacity under low phosphorus load. Environ Res 2023;238(Pt 2):117237.

[27] Ren Y, Yu G, Shi C, Liu L, Guo Q, Han C, et al. Majorbio Cloud: a one-stop, comprehensive bioinformatic platform for multiomics analyses. iMeta 2022;1(2):e12.

[28] Wu L, Ning D, Zhang B, Li Y, Zhang P, Shan X, et al. Author correction: global diversity and biogeography of bacterial communities in wastewater treatment plants. Nat Microbiol 2019;4(12):2579.

[29] Yu J, Xiao K, Xu H, Li Y, Xue Q, Xue W, et al. Spectroscopic fingerprints profiling the polysaccharide/protein/humic architecture of stratified extracellular polymeric substances (EPS) in activated sludge. Water Res 2023;235:119866.

[30] Morgan JW, Forster CF, Evison L. A comparative study of the nature of biopolymers extracted from anaerobic and activated sludges. Water Res 1990;24(6):743–50.

[31] Beal J, Farny NG, Haddock-Angelli T, Selvarajah V, Baldwin GS, Buckley-Taylor R, et al. Robust estimation of bacterial cell count from optical density. Commun Biol 2020;3(1):512.

[32] Zhou H, Zhang Y, Long CP, Xia X, Xue Y, Ma Y, et al. A citric acid cycle-deficient Escherichia coli as an efficient chassis for aerobic fermentations. Nat Commun 2024;15(1):2372.

[33] Jensen MB, Ottosen LDM, Kofoed MVW. H2 gas-liquid mass transfer: a key element in biological power-to-gas methanation. Renew Sustain Energy Rev 2021;147:111209.

[34] Ye F, Peng G, Li Y. Influences of influent carbon source on extracellular polymeric substances (EPS) and physicochemical properties of activated sludge. Chemosphere 2011;84(9):1250–5.

[35] More TT, Yadav JS, Yan S, Tyagi RD, Surampalli RY. Extracellular polymeric substances of bacteria and their potential environmental applications. J Environ Manage 2014;144:1–25.

[36] Chen X, Kong F, Fu Y, Si C, Fatehi P. Improvements on activated sludge settling and flocculation using biomass-based fly ash as activator. Sci Rep 2019;9(1):14590.

[37] Sheng GP, Yu HQ, Li XY. Extracellular polymeric substances (EPS) of microbial aggregates in biological wastewater treatment systems: a review. Biotechnol Adv 2010;28(6):882–94.

[38] Wang W, Yan Y, Zhao Y, Shi Q, Wang Y. Characterization of stratified EPS and their role in the initial adhesion of anammox consortia. Water Res 2020;169:115223.

[39] Wei Z, Huang S, Zhang Y, Li H, Zhou S. Characterization of extracellular polymeric substances produced during nitrate removal by a thermophilic bacterium Chelatococcus daeguensis TAD1 in batch cultures. RSC Adv 2017;7(70):44265–71.

[40] Pang Y, Wang J. Various electron donors for biological nitrate removal: a review. Sci Total Environ 2021;794:148699.

[41] Tian M, Zhao F, Shen X, Chu K, Wang J, Chen S, et al. The first metagenome of activated sludge from full-scale anaerobic/anoxic/oxic (A2O) nitrogen and phosphorus removal reactor using Illumina sequencing. J Environ Sci 2015;33:181–90.

[42] Lu H, Chandran K, Stensel D. Microbial ecology of denitrification in biological wastewater treatment. Water Res 2014;64:237–54.

[43] Li P, Wang Y, Zuo J, Wang R, Zhao J, Du Y. Nitrogen removal and N2O accumulation during hydrogenotrophic denitrification: influence of environmental factors and microbial community characteristics. Environ Sci Technol 2017;51(2):870–9.

[44] Wu J, Wang X, Fu Y, Yu Z, Meng F. Recruiting high-efficiency denitrifying consortia using Pseudomonas aeruginosa. Water Res 2025;277:123303.

[45] Ross-Gillespie A, Dumas Z, Kümmerli R. Evolutionary dynamics of interlinked public goods traits: an experimental study of siderophore production in Pseudomonas aeruginosa. J Evol Biol 2015;28(1):29–39.

[46] Goodell JW, Ben Jabeur S, Saâdaoui F, Nasir MA. Explainable artificial intelligence modeling to forecast bitcoin prices. Int Rev Financ Anal 2023;88:102702

[47] Aguilera-Campos KI, Stairs CW. Hydrogen metabolism: a eukaryote taps into the electron sink. Curr Biol 2022;32(1):R49–51.

[48] Greening C, Biswas A, Carere CR, Jackson CJ, Taylor MC, Stott MB, et al. Genomic and metagenomic surveys of hydrogenase distribution indicate H2 is a widely utilised energy source for microbial growth and survival. ISME J 2016;10(3):761–77.

[49] Bordel S, Martín-González D, Börner T, Muñoz R, Santos-Beneit F. Genome-scale metabolic model of the versatile bacterium Paracoccus denitrificans Pd1222. mSystems 2024;9(2):e0107723.

[50] Liu Z, Wang K, Chen Y, Tan T, Nielsen J. Third-generation biorefineries as the means to produce fuels and chemicals from CO2. Nat Catal 2020;3(3):274–88.

[51] Huang Q, Alengebawy A, Zhu X, Raza AF, Chen L, Chen W, et al. Performance of Paracoccus pantotrophus MA3 in heterotrophic nitrification-anaerobic denitrification using formic acid as a carbon source. Bioprocess Biosyst Eng 2022;45(10):1661–72.

[52] Kong L, Feng Y, Zheng R, Wu X, Mao Y, Sun J, et al. Interspecies hydrogen transfer between cyanobacteria and symbiotic bacteria drives nitrogen loss. Nat Commun 2025;16(1):5078.

[53] Hosmer J, McEwan AG, Kappler U. Bacterial acetate metabolism and its influence on human epithelia. Emerg Top Life Sci 2024;8(1):1–13.

[54] Wei W, Isobe K, Nishizawa T, Zhu L, Shiratori Y, Ohte N, et al. Higher diversity and abundance of denitrifying microorganisms in environments than considered previously. ISME J 2015;9(9):1954–65.

[55] Roothans N, van Loosdrecht MCM, Laureni M. Metabolic labour division trade-offs in denitrifying microbiomes. ISME J 2025;19(1):wraf020.

[56] Arai H. Regulation and function of versatile aerobic and anaerobic respiratory metabolism in Pseudomonas aeruginosa. Front Microbiol 2011;2:103.

[57] Frostegård Å, Vick SHW, Lim NYN, Bakken LR, Shapleigh JP. Linking meta-omics to the kinetics of denitrification intermediates reveals pH-dependent causes of N2O emissions and nitrite accumulation in soil. ISME J 2022;16(1):26–37.

[58] Jarman OD, Biner O, Wright JJ, Hirst J. Paracoccus denitrificans: a genetically tractable model system for studying respiratory complex I. Sci Rep 2021;11(1):10143.

[59] Strohm TO, Griffin B, Zumft WG, Schink B. Growth yields in bacterial denitrification and nitrate ammonification. Appl Environ Microbiol 2007;73(5):1420–24.

[60] Kim YJ, Lee HS, Kim ES, Bae SS, Lim JK, Matsumi R, et al. Formate-driven growth coupled with H(2) production. Nature 2010;467(7313):352–5.

[61] Jiang M, Zheng X, Chen Y. Enhancement of denitrification performance with reduction of nitrite accumulation and N2O emission by Shewanella oneidensis MR-1 in microbial denitrifying process. Water Res 2020;169:115242.

[62] Mulkidjanian AY, Makarova KS, Galperin MY, Koonin EV. Inventing the dynamo machine: the evolution of the F-type and V-type ATPases. Nat Rev Microbiol 2007;5(11):892–9.

[63] Mason-Jones K, Breidenbach A, Dyckmans J, Banfield CC, Dippold MA. Intracellular carbon storage by microorganisms is an overlooked pathway of biomass growth. Nat Commun 2023;14(1):2240.

[64] Yu HQ. Molecular insights into extracellular polymeric substances in activated sludge. Environ Sci Technol 2020;54(13):7742–50.

[65] Trunk K, Benkert B, Quäck N, Münch R, Scheer M, Garbe J, et al. Anaerobic adaptation in Pseudomonas aeruginosa: definition of the Anr and Dnr regulons. Environ Microbiol 2010;12(6):1719–33.

[66] Tao X, Zou K, Yuan M, Wen Y, Liu B, Qing T, et al. Beyond denitrification: alginate production by mucoid Pseudomonas aeruginosa using wastewater nitrate as electron acceptor. J Environ Chem Eng 2024;12(5):113679.

[67] Wang D, Ye W, Wu G, Li R, Guan Y, Zhang W, et al. Greenhouse gas emissions from municipal wastewater treatment facilities in China from 2006 to 2019. Sci Data 2022;9(1):317.

[68] Li H, Cao X, Liu Y, Shao Y, Nan Z, Teng L, et al. Safety of hydrogen storage and transportation: an overview on mechanisms, techniques, and challenges. Energy Rep 2022;8:6258–69.

[69] Zheng T, Liu C, Guo C, Zhang M, Li X, Jiang Q, et al. Copper-catalysed exclusive CO2 to pure formic acid conversion via single-atom alloying. Nat Nanotechnol 2021;16(12):1386–93.

[70] Cotton CAR, Claassens NJ, Benito-Vaquerizo S, Bar-Even A. Renewable methanol and formate as microbial feedstocks. Curr Opin Biotechnol 2020;62:168–80.

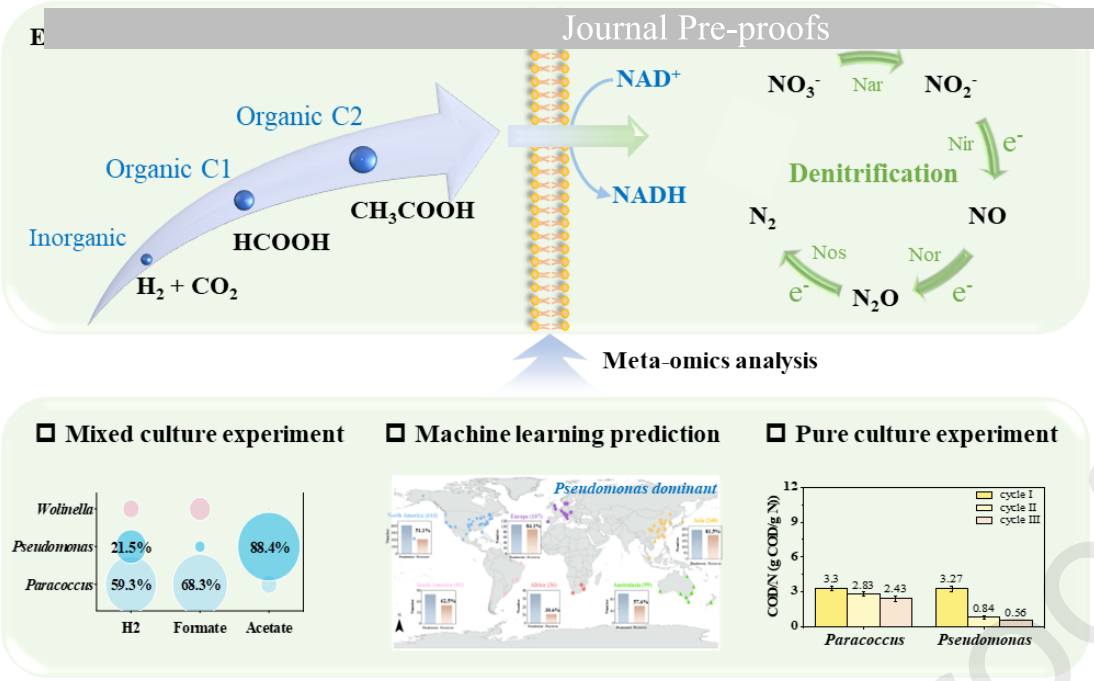

Highlights

- Formate and H_2-driven denitrification share similar microflora, dominated by *Paracoccus*.
- *Pseudomonas* dominates acetate-driven denitrification and is correlated with N removal.
- *Pseudomonas aeruginosa* is an energy-efficient microbe that utilizes less acetate.
- Constructed metabolic pathways of H_2, formate, and acetate in denitrification.

Declaration of Interest Statement

☒ The authors declare that they have no known competing financial interests or personal relationships that could have appeared to influence the work reported in this paper.

☐ The author is an Editorial Board Member/Editor-in-Chief/Associate Editor/Guest Editor for this journal and was not involved in the editorial review or the decision to publish this article.

☐ The authors declare the following financial interests/personal relationships which may be considered as potential competing interests:

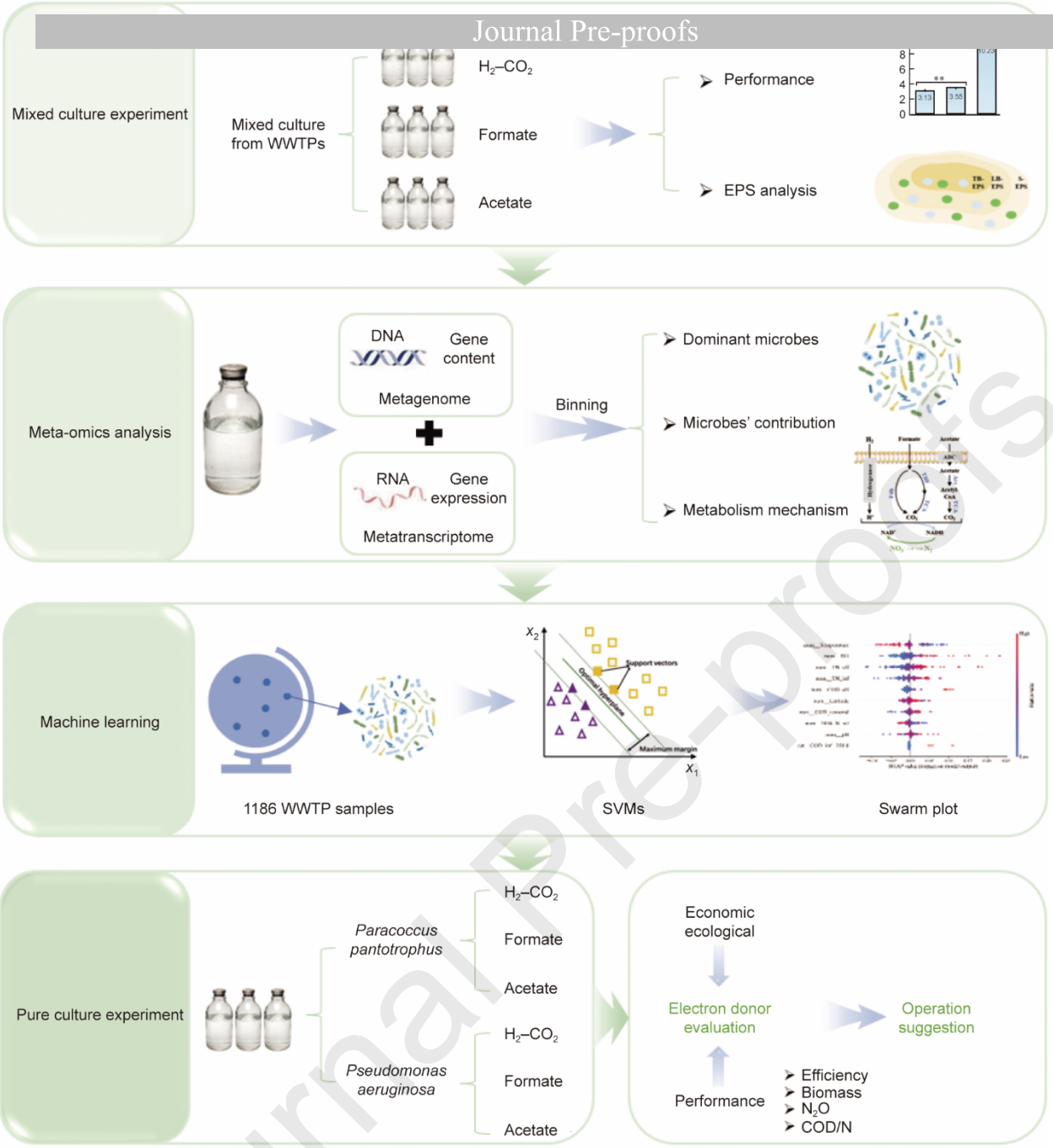

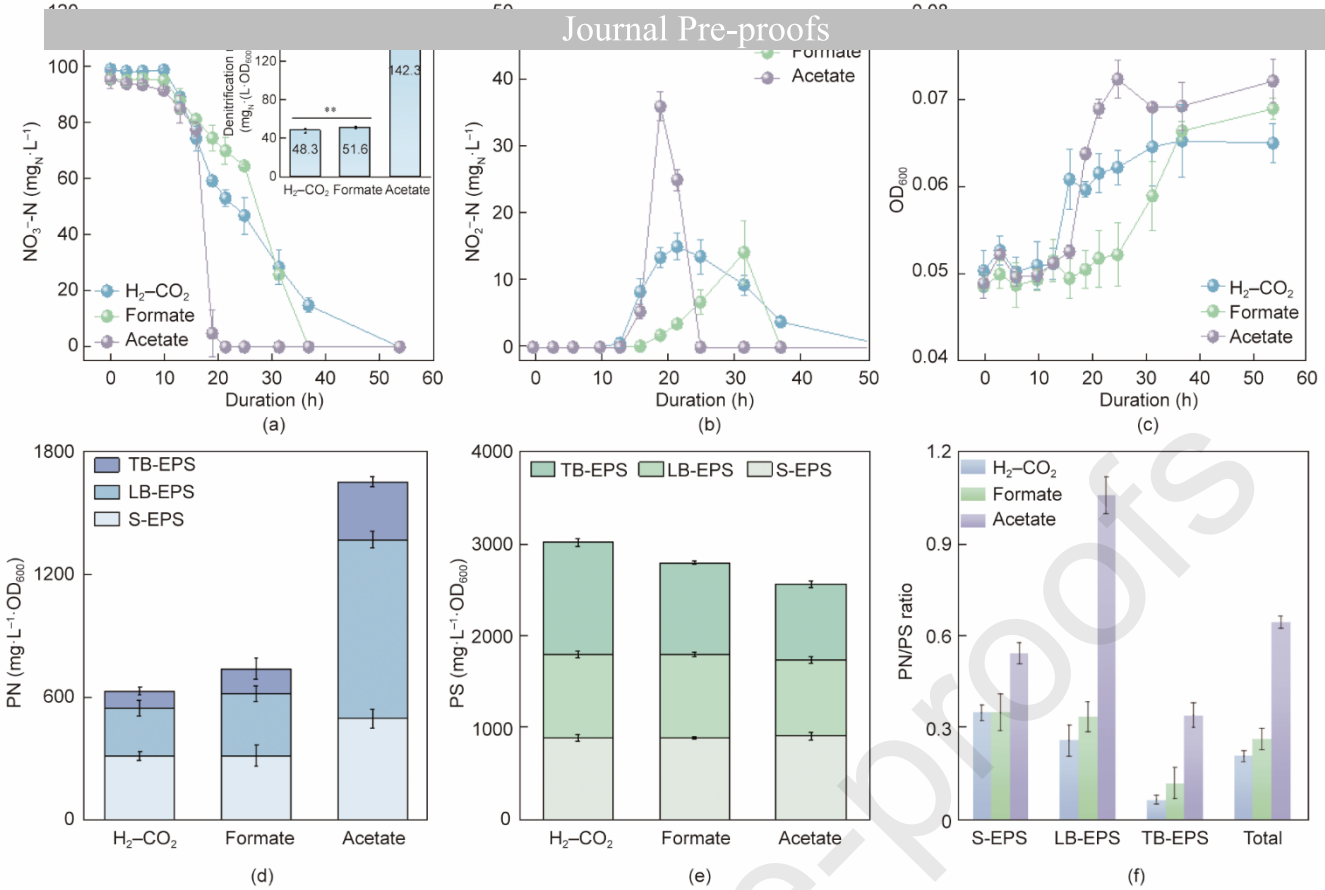

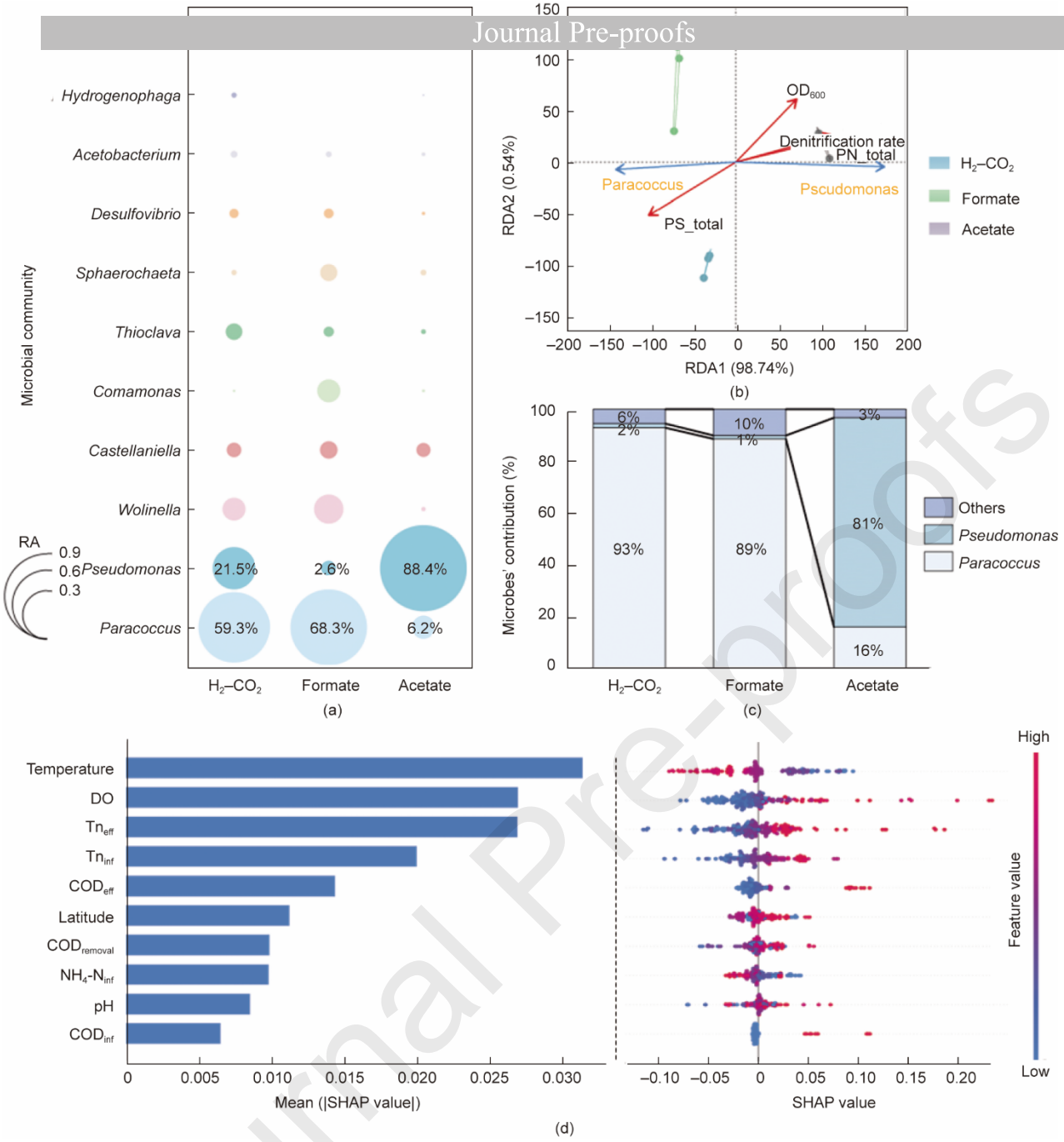

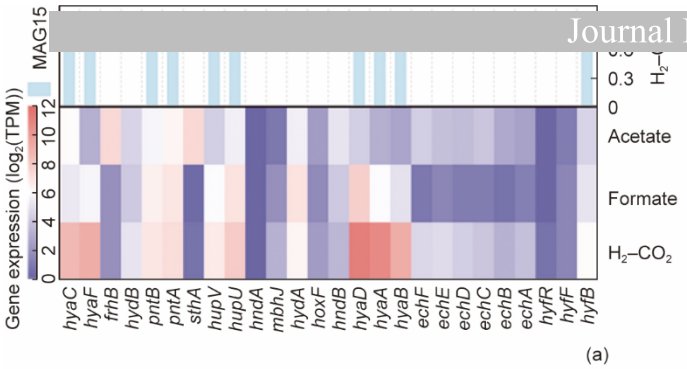

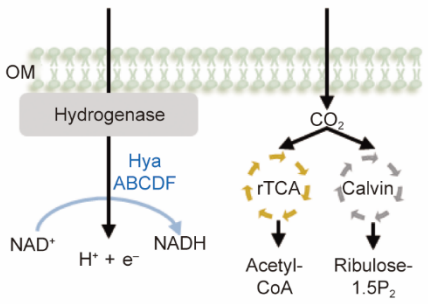

(a)

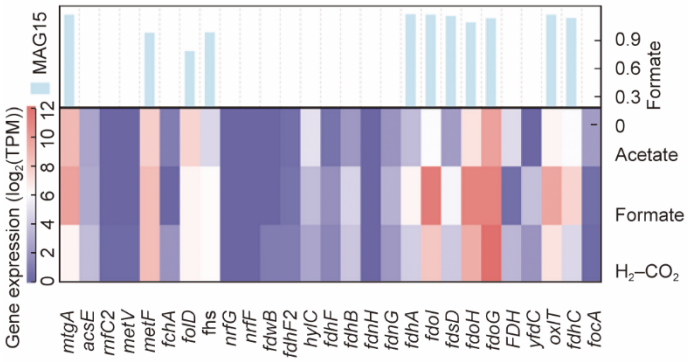

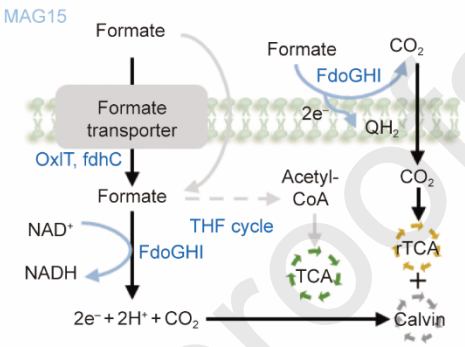

(b)

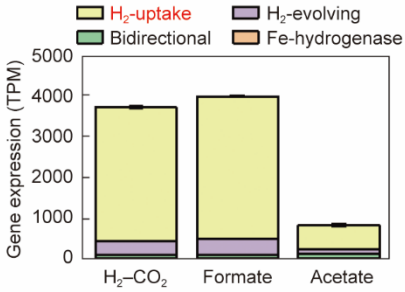

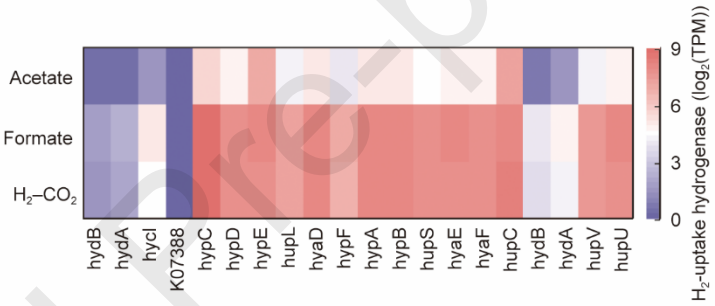

(c)

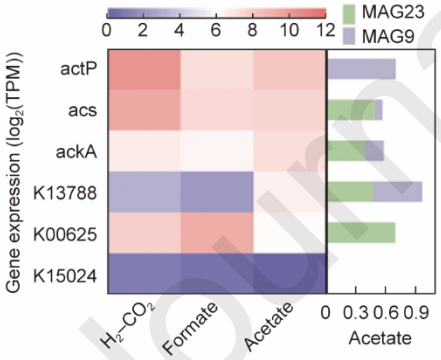

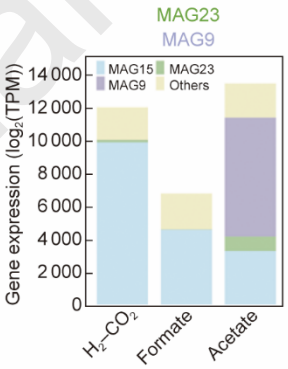

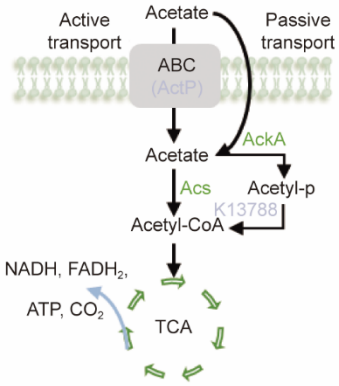

(d)

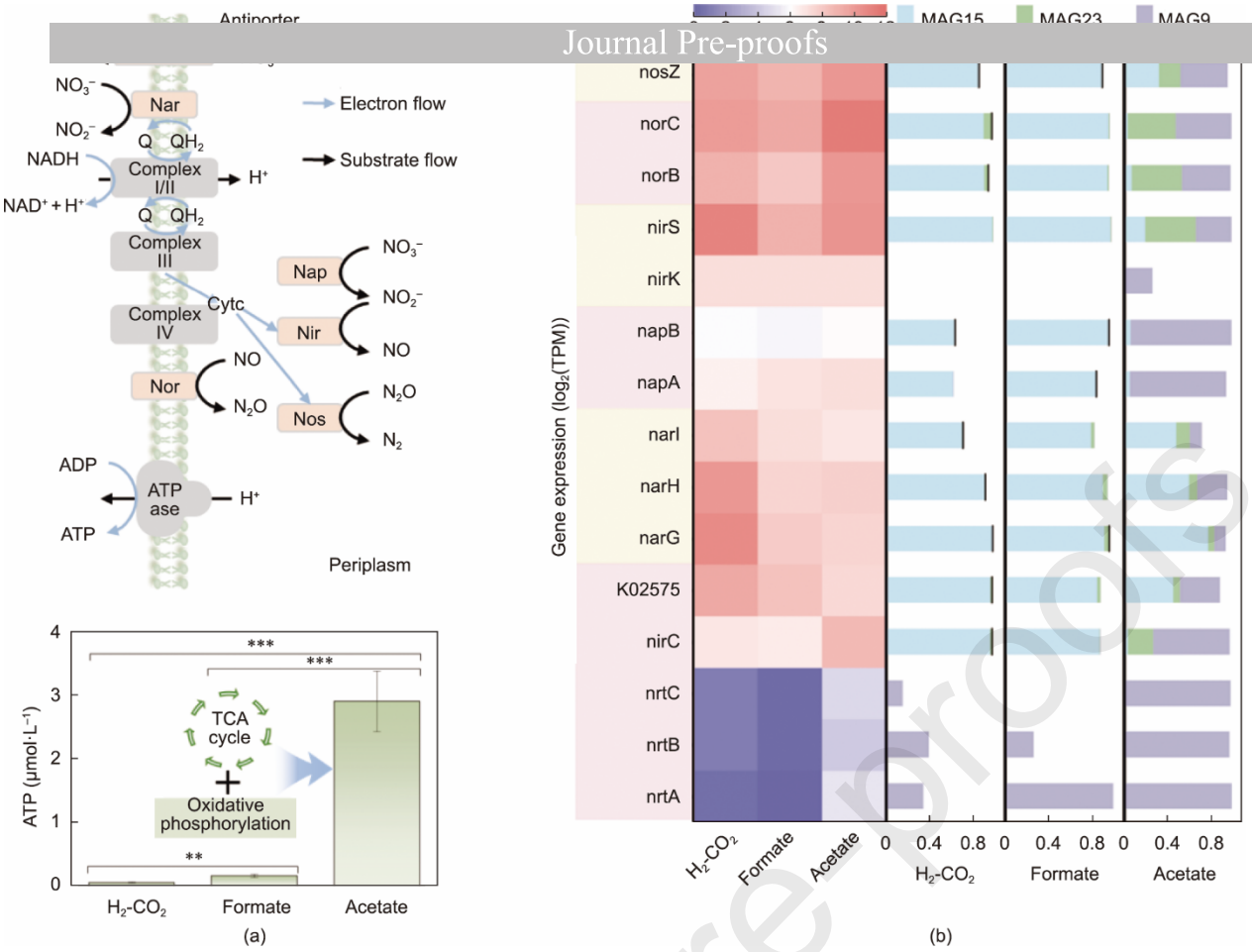

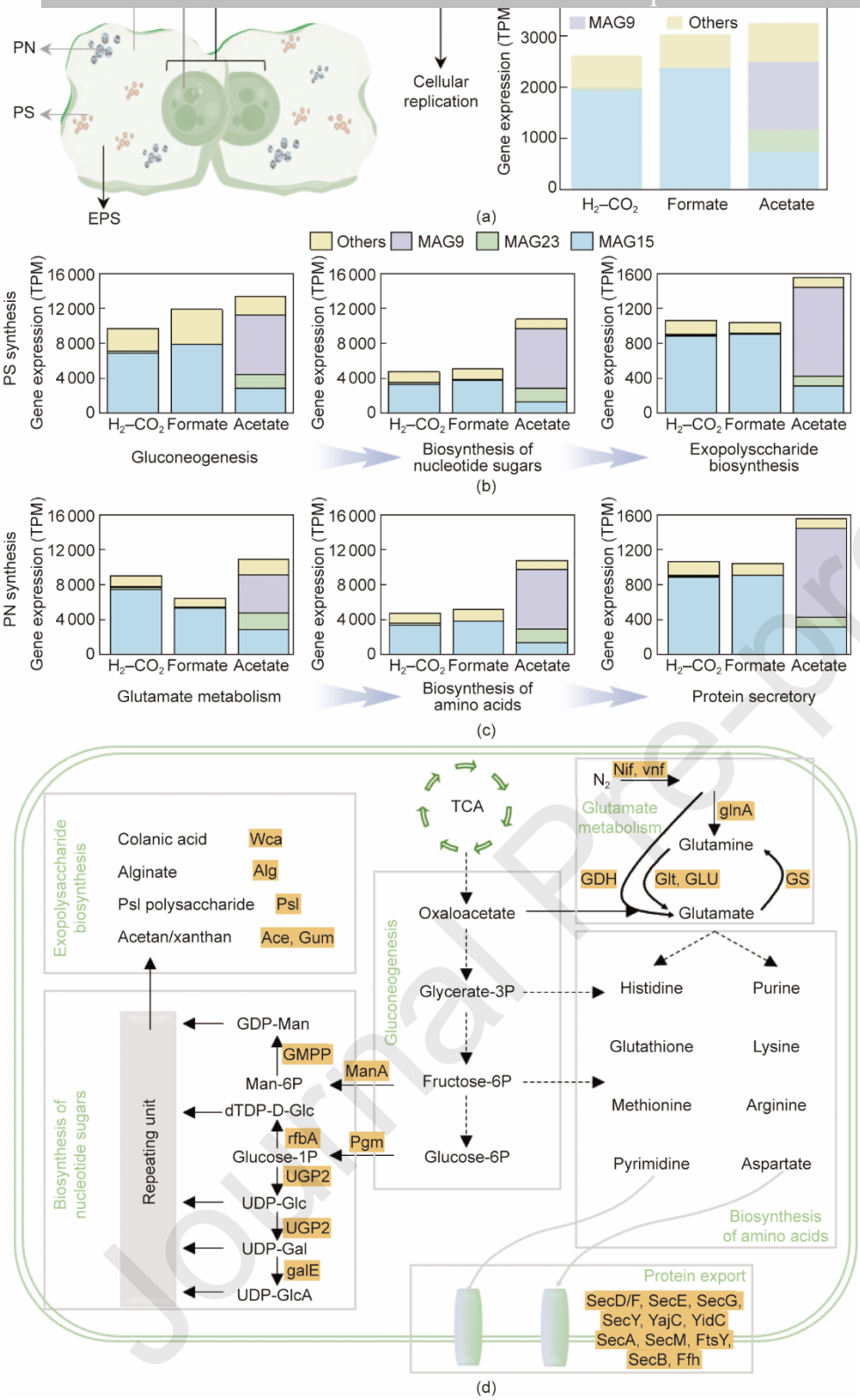

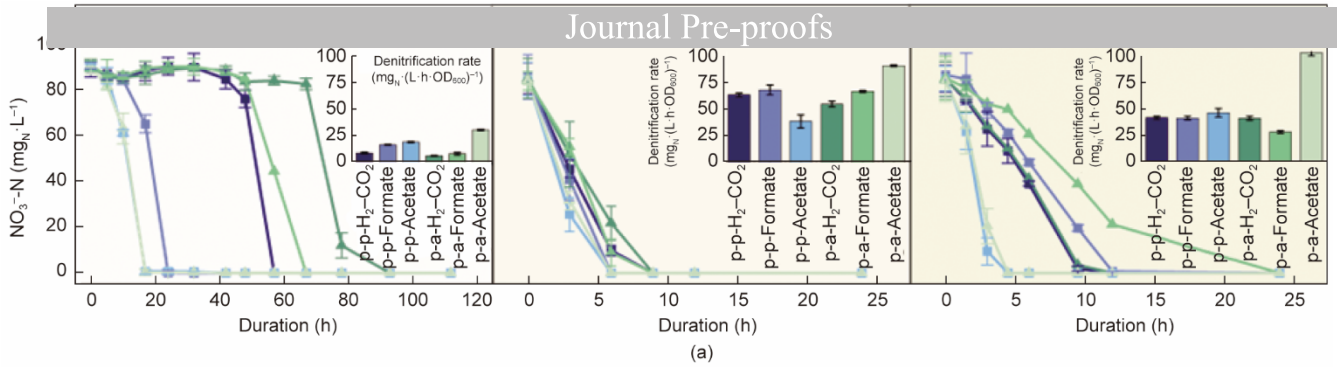

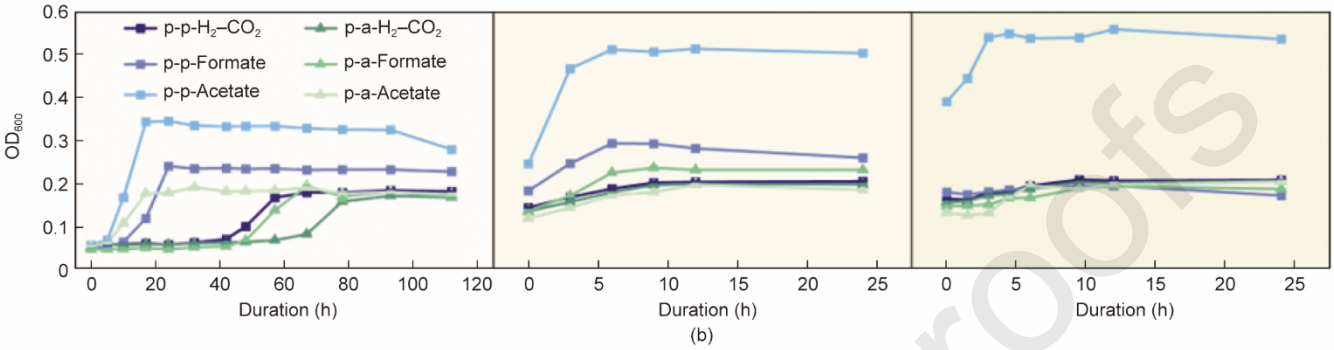

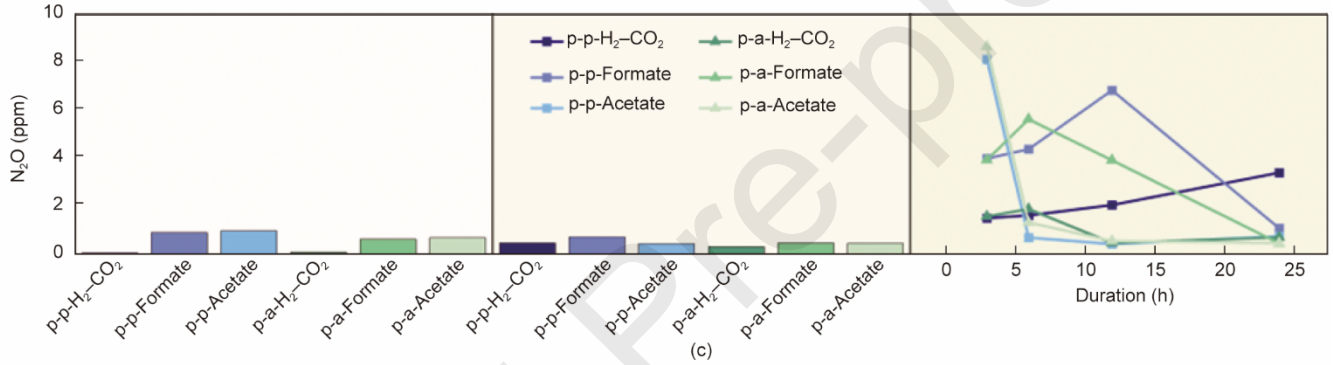

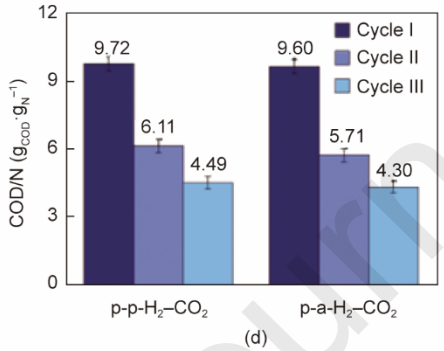

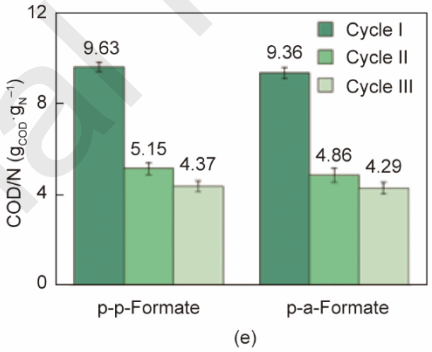

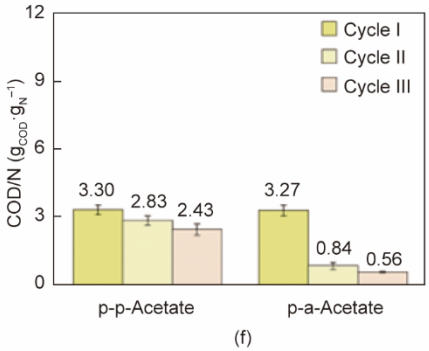

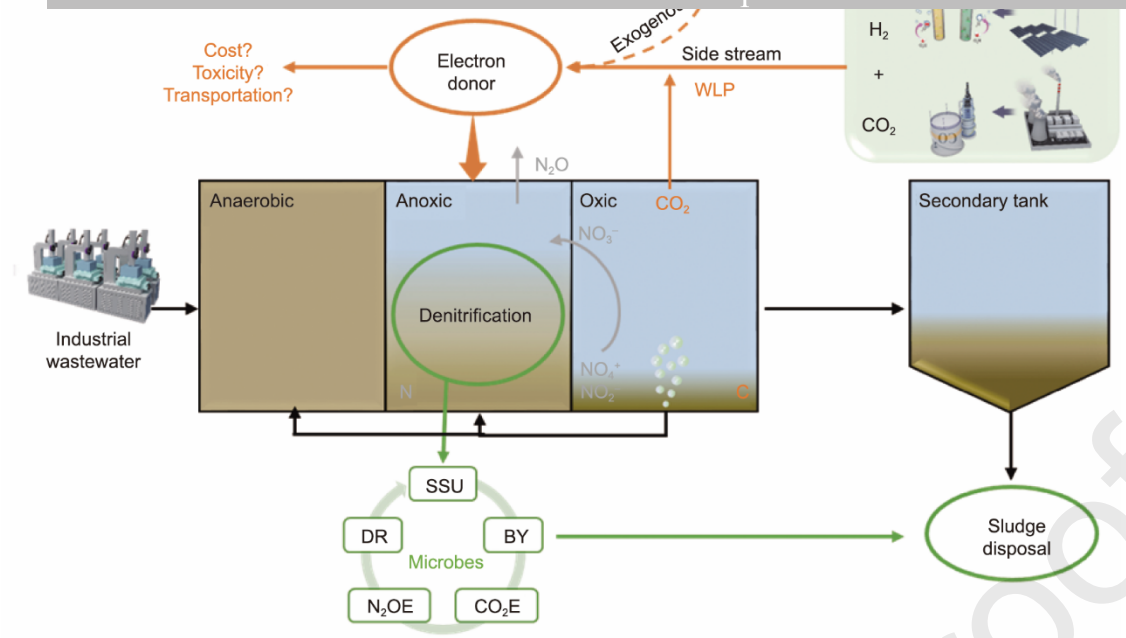

(a)

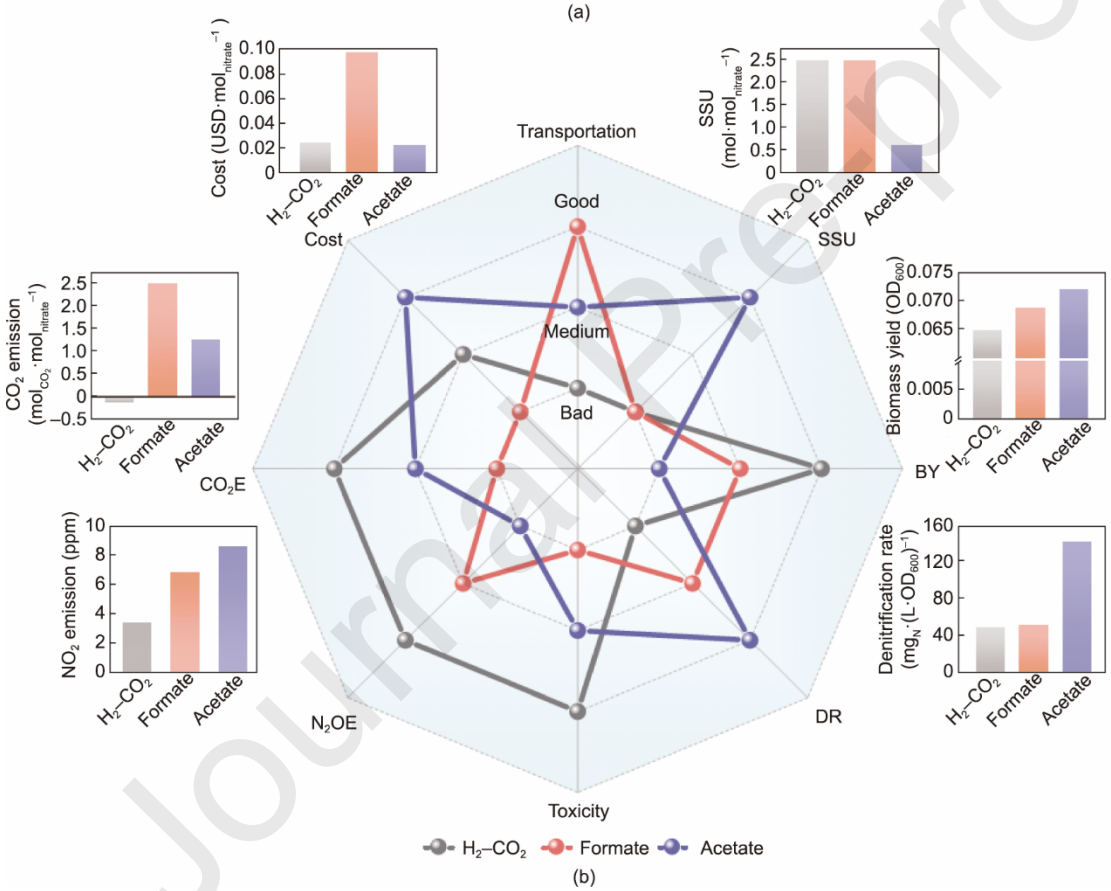

(b)